INVESTIGATION ON BALL SKIDDING AND TRACTION WITHIN ELASTOHYDRODYNAMIC FILMS

By

SHU-HSING CHEN

A DISSERTATION PRESENTED TO THE GRADUATE SCHOOL
OF THE UNIVERSITY OF FLORIDA IN PARTIAL FULFILLMENT
OF THE REQUIREMENTS FOR THE DEGREE OF
DOCTOR OF PHILOSOPHY

UNIVERSITY OF FLORIDA

1989

ACKNOWLEDGEMENTS

The author wishes to express his appreciation to Dr. D. Dareing, chairman of the supervisory committee, for his guidance and assistance in the investigation and for his suggestions in the preparation of this dissertation. Genuine thanks are extended to Dr. J. Tlusty, member of the supervisory committee, for his thoughtful advice.

The help and assistance of Kandiah Sivakumaran and the staff of the Machine Tool Laboratory are appreciated.

Special thanks and appreciation are extended to his wife, Shiow-Huey, for her constant support, encouragement, and understanding through the length of his program.

TABLE OF CONTENTS

LIST OF TABLES

LIST OF FIGURES

NOMENCLATURE

a	semi-major axis of Hertzian contact ellipse (mm)
b	semi-minor axis of Hertzian contact ellipse (mm)
d_p	bearing pitch diameter (mm)
d_b	ball diameter (mm)
E	elastic modulus (N/m^2)
E	convection factor = $\rho c\ V\ z^2/2\ k\ \Delta y$
E_1	complete elliptic integral of the first kind
E_2	complete elliptic integral of the second kind
F	external force on a bearing (N)
f_i, f_o	curvature factors $f_i \cdot D_b$ is the radius of inner race curvature $f_o \cdot D_b$ is the radius of outer race curvature
F_c	centrifugal force (N)
$\dot{H}$	heat generation rate (Watt)
h	film thickness (m or μm)
J	moment of inertia ($kg\text{-}m^2$)
K	ball/race contact stiffness ($N/mm^{1.5}$)
M_g	gyroscopic moment (N-m)
M_s	moment created by ball spinning (N-m)

m	mass (kg)
p	pressure (Pa)
Q	load on a rolling element (N)
q	load on each slice of the contact area (N)
r_p	radius of the pitch circle (mm)
u,v,w	velocities in x,y, and z directions respectively (m/sec)
X,R,ϕ	inertial coordinates describing the ball center
X,Y,Z	inertial coordinates describing the inner race center
$\bar{x},\bar{y},\bar{z}$	coordinate system for the contact area: $\bar{x}$ is transverse to the rolling direction; $\bar{y}$ is along the rolling direction; and $\bar{z}$ is normal to the contact area
α	contact angle (degree), or viscosity-pressure factor (1/Pa)
β	viscosity-temperature factor (1/°C)
δ	deflection (mm)
δ_{px}	axial preload (mm)
δ_{pr}	radial preload (mm)
η	lubricant dynamic viscosity (N-sec/m^2)
κ	ellipticity factor, $\kappa = a/b$
μ	coefficient of friction (or called traction coefficient for elastohydrodynamic lubrication)
τ	shear stress in elastohydrodynamic film (N/m^2)

θ	temperature (°C)
$\dot{\phi}_{ir}$	inner race rotating speed (rad/sec)
$\dot{\phi}_b$	ball orbiting speed about the bearing center (rad/sec)
ν	Poisson's ratio
$\omega_x, \omega_y, \omega_z$	ball rotating speeds about its own axis (rad/sec)
ω_s	spinning component of the relative ball/race rotating velocity (rad/sec)
ω_r	rolling component of the relative ball/race rotating velocity (rad/sec)

Subscripts:

b	refers to ball
i	refers to ball/inner race contact
ir	refers to inner race
o	refers to ball/outer race contact
or	refers to outer ring
s	refers to spinning or sliding

UNIT CONVERSION

Force:

1 lb_f = 4.448 N

Pressure:

1 Pa (Pascal) = 1 N/m^2

1 psi = 1 lb_f/in^2 = 6894.76 N/m^2

1 GPa = 1 x 10^9 Pa

Kinematic Viscosity:

1 centi-Stoke = 1 mm^2/sec

Dynamic Viscosity:

1 centi-poise = 10^{-3} Pa·sec

Power:

1 Watt = 1 Joule/sec = 1 N·m/sec

1 hp= 745.7 Watt

1 Btu/hr = 0.293 Watt

Abstract of Dissertation Presented to the Graduate School of the University of Florida in Partial Fulfillment of the Requirements for the Degree of Doctor of Philosophy

INVESTIGATION ON BALL SKIDDING AND TRACTION WITHIN ELASTOHYDRODYNAMIC FILMS

By

SHU-HSING CHEN

December 1989

Chairman: Donald W. Dareing
Major Department: Mechanical Engineering

In order to understand the sudden failure phenomenon in angular contact ball bearings, a time-simulation analysis which solves the equations of motion for each ball is performed. The analysis is performed on a 60° contact angle, 90 mm bore ball bearing which has failed (in a sudden manner) at 9,000 rpm during a test run. The calculation shows that the heat generation rate in this bearing increases significantly when the bearing speed exceeds a certain threshold value. This sudden increase of heat generation rate results from ball skidding caused by the gyroscopic moment effect. It was also found that a radial load on the bearing can induce an even higher heat generation rate, and this radial load effect can be solved by the time-simulation method. For comparison

reasons, the heat generation rate in a 15° contact angle ball bearing with the same dimensions is also calculated.

It has also been identified that the onset of the ball skidding is dependent on the friction in ball-race contacts, which are usually lubricated by elastohydrodynamic (EHD) films. The traction coefficients of EHD films are dependent on the sliding speed. Three different traction curves (curves describing traction-sliding relationship) are used in the analysis of ball motion and heat generation. It was found that traction coefficients in the thermal region are important to the onset of ball skidding, due to ball spinning which occurs in an angular contact ball bearing.

CHAPTER 1
INTRODUCTION

Scope of the Problem

Prediction of bearing speed limit is a problem of practical significance. In addition to the centrifugal loading, various dynamic effects may also limit the bearing speed. A particular dynamic effect which must be considered in the application of angular contact ball bearings the ball skidding caused by the gyroscopic moment effect.

The gyroscopic moment is generated because the ball self-rotational axis and the ball orbiting axis in an angular contact ball bearing are not parallel. Ball skidding occurs when the gyroscopic moment exceeds the friction torque provided by the ball-race contacts. The so-called minimum preload condition as shown below is developed from the above fact [1,2].

$$M_g < \mu D (Q_i + Q_o) \qquad (1\text{-}1)$$

where M_g is the gyroscopic moment, D is the ball diameter, Q_i and Q_o are loads on the inner and outer race contacts respectively, and μ is the traction coefficient.

To calculate the heat generation rate resulting from the ball skidding and to understand the causes of sudden bearing failure, however, a computer analysis is required. Furthermore, special care has to be taken in determining the traction coefficient in Eq.(1-1), not only because the elastohydrodynamic (EHD) traction behavior is complicated but also because there is another sliding motion, ball spinning, occurring in the bearing at the same time.

Literature Review

Methods of Bearing Analysis

The simplest method for calculating the ball motion (kinematic velocities) and the corresponding heat generation rate is to use the race-control theory, which, however, does not consider a balance of forces. The race-control theory was proposed by Jones [3].

Harris [1,2] was the first to present a computer method which considers the force actions in the calculation of bearing kinematics. Harris' method is now known as the quasi-static method. After Harris, two large-scale programs, CYBEAN [4] and SHABERTH [5], were developed based on the quasi-static method. However, the quasi-static method, which solves the equilibrium conditions for each ball as it fixed at a certain position in the bearing, is only valid when the bearing is axisymmetrically loaded.

An improved method for solving bearing dynamics was proposed by Walters [6] and Gupta [7,8]. Their method was to solve the equations of motion by time simulation. By using the time-simulation method, the time-cycle variation of the loads and contact angles of a ball in a radially loaded bearing can be calculated.

Sudden bearing failure caused by dynamic effects has been the subject of many bearing analyses. Besides the gyroscopic moment effect, some other effects also can cause sudden failure in bearings including radial bearings. For example, at high speeds, the centrifugal force may unload the ball-inner race contacts and the drag resulting from the lubricant in the bearing cavity can cause another type of ball skidding (different from that caused by the gyroscopic moment effect) [9,10,11]. Cage instability is another example. At high speeds, the smallest unbalance in the cage can lead to significant ball-cage interactions. Also, when the cage goes into whirl motion (a self-excited type of vibration) [12,13,14], significant sliding can be induced. However, due to the difficulty, only a few papers have reported experimental observation on the ball motion [15,16].

Elastohydrodynamic Lubrication Properties

In a rolling bearing, the high contact pressure prohibits the development of a convectional hydrodynamic film. However, a special form of fluid-film lubrication, elastohydrodynamic

lubrication, is able to develop between the balls and race of a bearing. The existence of the EHD film is attributable to the elastic deformation which creates a coherent channel for the fluid flow. Two particular issues in EHD lubrication are of concern in this research: (1) the effects of sliding (including ball spinning) on the EHD films and (2) the calculation of the EHD traction coefficient.

First, it was found by Cheng and Sternlight [17] that sliding (including spinning) has only a modest effect on the film thickness. The significance of this finding is that the isothermal film thickness formulas are applicable in cases where sliding is present. These isothermal film thickness formulas use the inlet viscosity to calculate the film thickness. It has also been suggested that although sliding does not significantly affect the EHD film thickness, the temperature rise caused by sliding can lead to lubricant deterioration through chemical reactions [19].

The second issue, the calculation of the traction coefficient, represents the most complicated aspect of the EHD phenomenon. Unlike the film thickness, the traction coefficient is sensitive to the sliding speed. It is now well accepted that the lubricant rheological behavior (determining traction force) can be described by the visco-elastic model and the limiting shear stress concept [20-23]. Experimental data on the rheological parameters, viscosity, shear modulus, and limiting shear stress are available for some common

lubricants [24,25,26]. Since the average pressure in the ball-race contact reaches 0.8 GPa, the lubricant traction behavior is governed by the non-Newtonian effect.

Objectives of Investigation

The first objective of the current research is to understand the ball skidding phenomenon (due to gyroscopic moment effect), especially how the ball skidding leads to sudden bearing failure and how the ball spinning affects the onset of ball skidding. Although much work on bearing dynamics has been performed, the ball skidding motion has never been clearly described. Most of the previous workers investigated bearings with small contact angles (less than 20°), where the gyroscopic moment effect is not as visible as it is on the bearings with large contact angles. Furthermore, some of these investigations were based on the quasi-static solution, which, as discussed earlier, is accurate only when the bearing is axisymmetrically loaded.

The second objective of this research is to study the relationship between the ball motion and the EHD traction behavior. This study needs to calculate the working temperature of the lubricant at the contacts and also needs to evaluate how the bearing performance responds to various traction curves. The ball skidding is a problem where the traction coefficient can strongly affect the ball motion.

Introduction to Current Methods

This research evaluates heat generation rates in a 15° and a 60° contact angle ball bearings (called Bearing A and Bearing B) to study the ball skidding phenomenon. The following methods are used:

1.The race-control theory is used in the following calculations: (1) heat generation caused by ball spinning; (2) initial conditions for time simulation; and (3) threshold speeds of ball skidding.

2.Both the quasi-static method and the time-simulation method are performed to calculate heat generation caused by ball skidding. The time-simulation method provides more accurate solutions for non-axisymmetrically loaded bearings.

3.A hypothetical traction curve (called Curve 1) which assumes the traction coefficient is almost independent of sliding speed (except in the linear region of the traction curve) is used in most of the calculations. Two other hypothetical traction curves (Curves 2 and 3) which simulate true EHD traction behavior are used to study which part of the traction curve really affects the onset of ball skidding.

4.Temperature rise in the EHD film caused by ball spinning is also presented. The temperatures on the solid boundaries of the EHD film are determined by modeling the solids as semi-infinite planes subjected to a moving heat source [27,28].

CHAPTER 2
MATHEMATICAL MODEL FOR BEARING ANALYSIS

Basic Equations and Coordinate Systems

The major purpose of bearing analysis in this work is to determine the heat generation in bearings. Such calculation is accomplished by solving the equations of motion for each bearing element (ball or race) to determine the relative motions between the elements.

Equations of Motions

According to Newton's law, the equations of motion are as follows:

for Cartesian coordinates (x,y,z),

$$\begin{aligned} m\,\ddot{x} &= \Sigma F_x \\ m\,\ddot{y} &= \Sigma F_y \\ m\,\ddot{z} &= \Sigma F_z \end{aligned} \tag{2-1}$$

for cylindrical coordinates (x,r,ϕ),

$$\begin{aligned} m\,\ddot{x} &= \Sigma F_x \\ m\,\ddot{r} &= \Sigma F_r \\ m\,r\,\ddot{\phi} + 2\,m\,\dot{r}\,\dot{\phi} &= \Sigma F_\phi \end{aligned} \tag{2-2}$$

If a body rotates with an angular velocity (ω_x, ω_y, ω_z) about a fixed point which rotates with an angular speed $\dot{\phi}$

about an axis parallel to the x-axis, the equation of motion can be written as

$$J\,\dot{\omega}_x = \Sigma M_x$$
$$J\,\dot{\omega}_y - J\,\omega_z\,\dot{\phi} = \Sigma M_y \qquad (2\text{-}3)$$
$$J\,\dot{\omega}_z + J\,\omega_y\,\dot{\phi} = \Sigma M_z$$

Note that for a ball, $J = J_x = J_y = J_z$.

Two Simplified Methods

Quasi-static method. The quasi-static model can be used when steady-state conditions prevail. This method neglects the inertial forces (induced by accelerations: $\ddot{x}$, $\ddot{y}$, $\ddot{z}$, $\ddot{r}$, $\ddot{\phi}$, $\dot{\omega}_x$, $\dot{\omega}_y$, and $\dot{\omega}_z$) and Coriolis force ($2\,m\,\dot{r}\,\dot{\phi}$) but considers the centrifugal force and gyroscopic moment. The equations used in this method are called force equilibrium equations.

Race-control theory. The race-control theory is based on a set of hypothetical kinematic constraints which provide a simplified method for solving for bearing kinematic velocities.

Coordinate Systems for Bearing Analysis

Ball bearings, except for some specially designed bearings, consist of an inner race, an outer race, a number of balls, and a cage. Three coordinate systems are defined to describe the position and motion of each of these elements. These coordinate systems are referred to as inertial coordinate system, ball-fixed coordinate system, and contact

coordinate system, respectively. These three coordinate systems are shown in Fig.2-1.

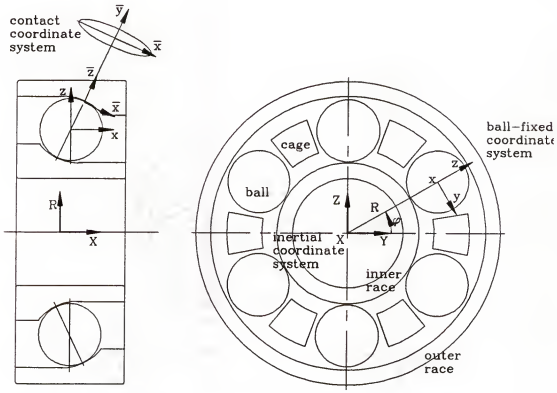

Figure 2-1 Coordinate systems for bearing analysis.

Inertial coordinate system. The inertial coordinate system is used to describe the position and motion (except for the self-rotation of the ball) of each bearing element. The race and cage are described by a set of rectangular coordinates, denoted as (X,Y,Z); the balls are described by a set of cylindrical coordinates, denoted (X,R,ϕ). The origin of this coordinate system, point O, is located at the center of the non-moving race. The X-axis is along the spindle axial direction.

In the inertial coordinate system, the following positions and velocities are defined:

for the balls,

(X_b, R_b, ϕ_b): coordinates of the ball center

$\dot{\phi}_b$: ball orbiting velocity about the reference point for the inner race,

(X_{ir}, Y_{ir}, Z_{ir}): coordinates of the inner race center

$\dot{\phi}_{ir}$: inner race rotating speed

Ball-fixed coordinate system. The ball-fixed coordinate system, denoted as (x,y,z), is attached to each ball center to describe the self-rotational motion of each ball. The x-axis of this coordinate system is parallel to the X-axis of the inertial coordinate system, and the z-axis points in the radial direction. The following velocities are defined in these coordinate systems:

ω_x, ω_y, ω_z: ball spinning speeds in the x, y, and z directions.

Contact coordinate system. The contact coordinate system is located at the center of each ball-race contact ellipse and is denoted as $(\bar{x}, \bar{y}, \bar{z})$. In this coordinate system, the $\bar{x}$-axis is transverse to the rolling direction, the $\bar{y}$-axis is along the rolling direction, and the $\bar{z}$-axis is normal to the contact. This coordinate system will be illustrated later.

Variables to be Solved

There are nine variables to be solved, six for the balls and three for the inner race (assuming the outer race is fixed). These are X_{ir}, Y_{ir}, and Z_{ir} for the inner race and X_b, R_b, ω_x, ω_y, ω_z, and $\dot{\phi}_b$ for each ball.

Sliding Motions in Ball Bearings

Most of the heat generated in a rolling bearing is due to sliding at ball-race contacts. There are four possible types of sliding motion which may occur in these contacts. The patterns of these four types of sliding are shown in Fig.2-2.

Ball Spinning

In angular contact ball bearings, the extensions of the two contact tangents (Lines L_i and L_o in Fig.2-3) do not intersect at the same point in the bearing axis. This means that angular contact ball bearings are prevented from a pure rolling condition. In effect, there is a relative spinning motion (ball spinning) between the ball and race in the contact area. The ball spinning friction will be further discussed later when methods of calculating bearing kinematic velocities are introduced.

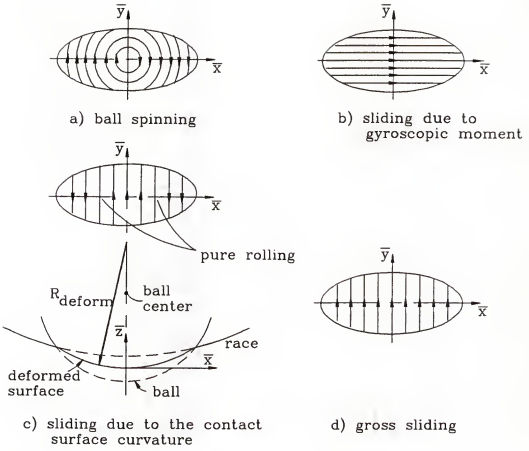

Figure 2-2 Sliding line patterns.

Sliding due to Gyroscopic Moment Effect

In an angular contact ball bearing the ball spinning axis is not parallel to the ball orbiting axis, as shown in Fig.2-4 (where a thrust ball bearing is shown). A moment, known as the gyroscopic moment, is required for the precession motion of balls (rotation of the ball spinning axis). The magnitude of the required gyroscopic moment is

$$M_g = J \dot{\phi}_b \omega_z$$

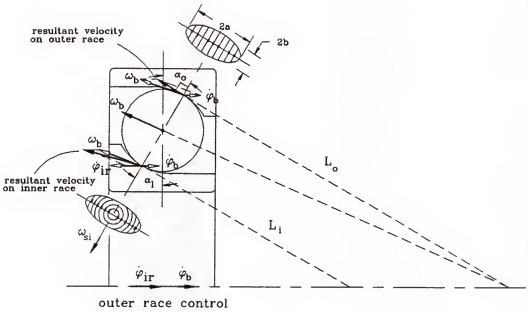

Figure 2-3 Race control theory and the sliding lines in ball-race contacts.

The required moment can be obtained from the friction forces at the ball-race contacts. If the friction forces do not provide a sufficient moment, the ball will rotate about its own y-axis and produce excessive sliding. The well-known minimum preload condition can be written as follows:

$$J\ \dot{\phi}_b\ \omega_z < 0.5\ \mu(u_{s\bar{x}})\ D_b\ (Q_i + Q_o) \qquad (2\text{-}4)$$

where $u_{s\bar{x}}$ is the sliding speed in the $\bar{x}$-direction (transverse to the rolling direction).

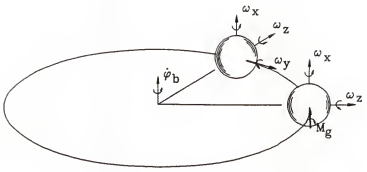

$$M_g = J_b \dot{\varphi}_b \omega_z$$

Figure 2-4 Gyroscopic moment in an angular contact ball bearing.

Sliding due to the Curvature of Contact Surface

As shown in Fig.2-2c, the contact area is a curved surface, thus distances from the ball spinning axis to individual points in the surface are different. Therefore, pure rolling occurs at most at two points. The middle section slides in one direction, and the outer sections slide in the opposite direction. For pure radial bearings, this sliding friction represents the major friction source.

Gross Sliding in Ball-Race Contacts

Normally, gross sliding does not occur in rolling bearings except due to the following reasons: ball skidding due to gyroscopic moment, ball skidding due to lubricant drag, acceleration or deceleration of bearings, and collision between cage and ball. The pattern of gross sliding is shown in Fig.2-2d.

Force Equilibrium Equations for Load Distribution Analysis

The load distribution in a bearing can be calculated by solving the force equilibrium equations (for steady-state loads), and an iterative method has to be used to solve these equations.

The force equilibrium equations for each ball (according to Fig.2-5) are as follows:

for x-direction,

$$Q_i \sin\alpha_i - Q_o \sin\alpha_o - \mu Q_i \cos\alpha_i + \mu Q_o \cos\alpha_o = 0 \quad (2\text{-}5a)$$

for z-direction,

$$Q_i \cos\alpha_i - Q_o \cos\alpha_o + \mu Q_i \sin\alpha_i - \mu Q_o \sin\alpha_o + F_c = 0 \quad (2\text{-}5b)$$

where F_c is the centrifugal force which can be calculated by

$$F_c = m_b R_b \dot{\phi}_b^2 \quad (2\text{-}6)$$

In Eq.(2-5a and b), the terms that include the coefficient of friction μ are the reaction moments against the gyroscopic moment. These terms are included to deal with the effects of gyroscopic moment on the load distribution. The coefficient of friction can be calculated from the following equation:

$$0.5 \mu d_b (Q_i + Q_o) = M_{gy} \quad (2\text{-}7)$$

where M_{gy} is the gyroscopic moment.

Assuming that the outer race is fixed, the equilibrium equations for the inner race are as follows:

$$F_x = \Sigma\, Q_i \sin\alpha_i \tag{2-8a}$$

$$F_y = \Sigma\, Q_i \cos\alpha_i \cos\phi_b \tag{2-8b}$$

$$F_z = \Sigma\, Q_i \cos\alpha_i \sin\phi_b \tag{2-8c}$$

In the above equations, the range of summation is the complete ball set. The calculation of the ball-race interaction forces (Q_i and Q_o) requires a complex contact geometry analysis and is discussed in Chapter 3.

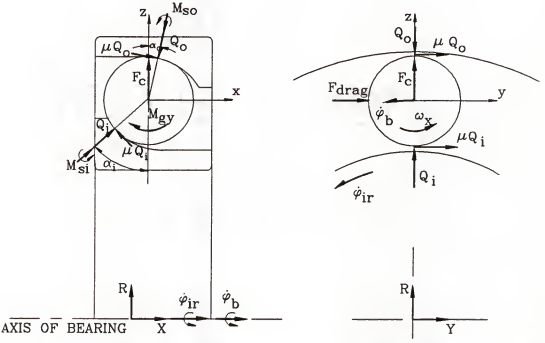

Figure 2-5 Forces and moments acting on a ball and the races (a simplified model).

Solving Bearing Kinematics by Using the Race-Control Theory

Race-Control Theory

Due to the fact that the ball self-rotational axis is not parallel to the bearing axis, the kinematics of angular contact ball bearings is somewhat more difficult than that of pure radial bearings. The simplest method to calculate the kinematics of this type of bearing is to use the race-control theory.

The race-control theory, which is developed from the concept of dry friction, assumes that the ball spinning only occurs on one of the races. The race on which no spinning occurs is called the controlling race (being the race that produces more resistance to spinning). Usually, the controlling race is the inner race at low speeds and the outer race at high speeds. The race-control theory provides an extra condition for solving the bearing kinematics. However, for bearings lubricated by EHD films, the race-control theory somewhat departs from the real situation because the relative spinning can occur on both races.

The case shown in Fig.2-3 is an outer race-control case where the ball self-rotational axis intersects Line L_o at the same point in the bearing axis. The resultant velocity of ball orbiting velocity, ball spinning velocity, and the outer race velocity (which is zero) is parallel to the contact surface, and there is no spinning on the outer race. For the inner

race, the net velocity is not parallel to the contact surface. The sliding lines caused by the relative spinning is also shown in the inner race contact while the sliding lines in the outer race represent the sliding due to the curved surface.

By utilizing the race-control theory, three equations can be written according to Fig.2-6. In the following equations, Eq.(2-9a) is written according to the no spinning condition in the controlling race; Eq.(2-9b) is written for the no gross sliding condition in the controlling race; Eq.(2-9c) is for the no gross sliding condition in the non-controlling race. In these equations, subscript c refers to the controlling race, and subscript n refers to the non-controlling race,

$$\sin\alpha_c \ \omega_x + \cos\alpha_c \ \omega_z + \sin\alpha_c \ \dot{\phi}_b = \dot{\phi}_{cr} \sin\alpha_c \qquad (2\text{-}9a)$$

$$0.5\, d_b \cos\alpha_c\, \omega_x - 0.5\, d_b \sin\alpha_c\, \omega_z + (r_p + 0.5\, d_b \cos\alpha_c)\, \dot{\phi}_b = (r_p + 0.5\, d_b \cos\alpha_c)\, \dot{\phi}_{cr} \qquad (2\text{-}9b)$$

$$0.5\, d_b \cos\alpha_n\, \omega_x - 0.5\, d_b \sin\alpha_n\, \omega_z + (r_p + 0.5\, d_b \cos\alpha_n)\, \dot{\phi}_b = (r_p + 0.5\, d_b \cos\alpha_n)\, \dot{\phi}_{nr} \qquad (2\text{-}9c)$$

where r_p is the radius of the pitch circle.

Calculation of Ball Spinning Friction

The following equations can be used to determine the ball spinning velocities and rolling velocities. The ball spinning velocities for the inner race and outer race are

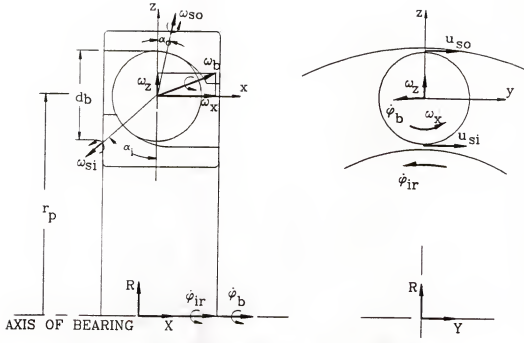

Figure 2-6 Rotational velocities in a ball bearing.

$$\omega_{si} = \omega_x \sin\alpha_i + \omega_z \cos\alpha_i + \dot{\phi}_b \sin\alpha_i - \dot{\phi}_{ir} \sin\alpha_i \quad (2\text{-}10a)$$

$$\omega_{so} = \omega_x \sin\alpha_o + \omega_z \cos\alpha_o + \dot{\phi}_b \sin\alpha_o \quad (2\text{-}10b)$$

The rolling velocities are

$$\omega_{ri} = \omega_x \cos\alpha_i - \omega_z \sin\alpha_i + \dot{\phi}_b \cos\alpha_i - \dot{\phi}_{ir} \cos\alpha_i \quad (2\text{-}11a)$$

$$\omega_{ro} = \omega_x \cos\alpha_o - \omega_z \sin\alpha_o + \dot{\phi}_b \cos\alpha_o \quad (2\text{-}11b)$$

A parameter which is often used to assess bearing performance is called spin-to-roll ratio. This ratio is defined as (for both inner race and outer race)

$$\text{spin-to-roll ratio} = \omega_s / \omega_r \quad (2\text{-}12)$$

The frictional moment caused by the ball spinning motion can be derived by integrating the moments produced by friction forces over the contact ellipse. If the pressure distribution in the contact area is Hertzian and the coefficient of friction is a constant, this frictional moment will be

$$M_s = \frac{3\mu Q a E_2}{8} \tag{2-13a}$$

where E_2 is the complete elliptic integral of second kind as defined in Appendix A, and a is the length of the semi-major axis.

The heat generation rate due to ball spinning can be calculated by

$$\dot{H} = M_{si}\ \omega_{si} + M_{so}\ \omega_{si} \tag{2-13b}$$

where subscripts i and o refer to inner race and outer race respectively.

Equations of Motion for a Ball

The race-control theory, which does not consider the actual force equilibrium conditions, has two drawbacks: (1) the ball spinning may occur on both races, and (2) the gyroscopic moment effect is not considered. This section presents another method which solves the equations of motion to determine bearing kinematic velocities.

Discretization of the Contact Area

Since sliding velocity, pressure, and coefficient of friction vary from point to point within a contact area, the frictional force and moment occurring in a contact must be calculated by integration over the contact area. For this reason, each contact area is divided into slices as shown in Fig.2-7. The following two assumptions are used in the discretization:

1. The contact area is discretized in the $\bar{x}$-direction only. This is because contact areas are often narrow ellipses.
2. Inside each slice the sliding velocity, pressure, and coefficient of friction are assumed to be constant, and their values for each slice are calculated at the center point of the slice.

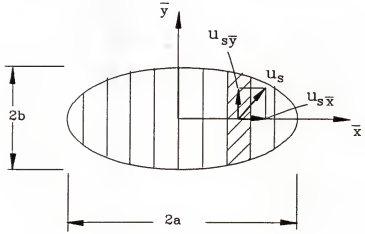

Figure 2-7 Discretization of the contact area for the calculation of sliding friction.

Deriving the Equations of Motion

To solve for the ball motion, the following four unknowns should be solved: $\dot{\phi}_b$, ω_x, ω_y, and ω_z. The equations of motion (four equations for each ball) which consider the effects of the inertial forces and inertial torques can be written by making use of Fig.2-8 as follows:

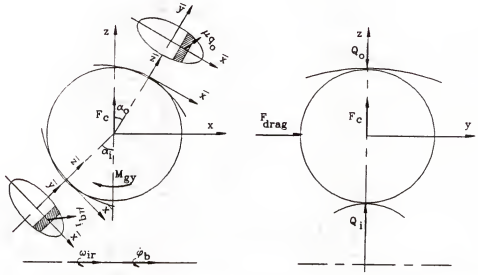

Figure 2-8 Forces and moments acting on a ball and the races.

forces in rolling direction,

$$m_b R_b \ddot{\phi}_b + 2 m_b \dot{R}_b \dot{\phi}_b = - \int \mu(u_{si}) \frac{u_{s\bar{y}i}}{u_{si}} q_i \, dA_i + \int \mu(u_{so}) \frac{u_{s\bar{y}o}}{u_{so}} q_o \, dA_o + F_{drag} + Q_{cage} \quad (2\text{-}14a)$$

where F_{drag} and Q_{cage} represent forces exerted by the lubricant and cage,

moments in the x-direction,

$$J_b \dot{\omega}_x = \int \mu(u_{si}) \frac{u_{s\bar{y}i}}{u_{si}} q_i \, r_{czi} \, dA_i + \int \mu(u_{so}) \frac{u_{s\bar{y}o}}{u_{so}} q_o \, r_{czo} \, dA_o \qquad (2\text{-}14b)$$

moments in the y-direction,

$$J_b \dot{\omega}_y - J_b \omega_z \dot{\phi}_b = -0.5 \, d_b \left[\int \mu(u_{si}) \frac{u_{s\bar{x}i}}{u_{si}} q_i \, dA_i + \int \mu(u_{so}) \frac{u_{s\bar{x}o}}{u_{so}} q_o \, r_{czo} \, dA_o \right] \qquad (2\text{-}14c)$$

moments in the z-direction,

$$J_b \dot{\omega}_z + J_b \omega_y \dot{\phi}_b = -\int \mu(u_{si}) \frac{u_{s\bar{y}i}}{u_{si}} q_i \, r_{cxi} \, dA_i + \int \mu(u_{so}) \frac{u_{s\bar{y}o}}{u_{so}} q_o \, r_{cxo} \, dA_o \qquad (2\text{-}14d)$$

In Eq.(2-14a to d),

$u_{s\bar{x}i}$, $u_{s\bar{x}o}$ = sliding speed in the $\bar{x}$-direction (for inner race and outer race)

$u_{s\bar{y}i}$, $u_{s\bar{y}o}$ = sliding speed in the $\bar{y}$-direction (for inner race and outer race)

$$u_{si} = \sqrt{u^2_{s\bar{x}i} + u^2_{s\bar{y}i}}$$

$$u_{so} = \sqrt{u^2_{sxo} + u^2_{syo}}$$

r_{czi}, r_{czo}, r_{cxi}, r_{cxo}: distances from a point in the contact area to the ball center (as indicated in Fig.2-9)

q: the load on each slice

Q: the total load on the whole contact

Now the sliding velocities have to determined.

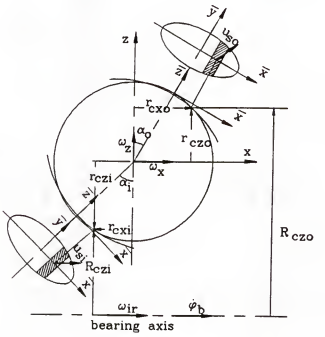

Figure 2-9 Geometric model for calculating sliding velocities.

Sliding Velocity on Each Slice

The sliding velocity at a point $(\bar{x},\bar{y},\bar{z})$ in a contact can be written as follows:

sliding in $\bar{x}$-direction,

$$u_{s\bar{x}i} = u_{s\bar{x}o} = 0.5\ \omega_y\ d_b \qquad (2\text{-}15a)$$

(this sliding velocity is caused by the gyroscopic moment) sliding in y-direction,

for inner race,

$$u_{s\bar{y}i} = \omega_x\ r_{czi} - \omega_z\ r_{czi} - \dot{\phi}_b\ R_{czi} + \dot{\phi}_{ir}\ R_{czi} \qquad (2\text{-}15b)$$

for outer race,

$$u_{s\bar{y}o} = -\omega_x\ r_{czo} + \omega_z\ r_{czo} - \dot{\phi}_b\ R_{czi} \qquad (2\text{-}15c)$$

The distances from the point at (x,y,z) to the ball center and the bearing axis can be derived as follows:

$$r_{cxi} = 0.5\ d_b\ \sin\alpha_i + \bar{x}\ \cos\alpha_i + \bar{z}\ \sin\alpha_i$$

$$r_{czi} = 0.5\ d_b\ \cos\alpha_i + \bar{x}\ \sin\alpha_i - \bar{z}\ \cos\alpha_i$$

$$R_{czi} = r_p - 0.5\ d_b\ \cos\alpha_i - \bar{x}\ \sin\alpha_i + \bar{z}\ \cos\alpha_i$$

$$r_{cxo} = 0.5\ d_b\ \sin\alpha_i + \bar{x}\ \cos\alpha_i + \bar{z}\ \sin\alpha_i$$

$$r_{czo} = 0.5\ d_b\ \cos\alpha_i + \bar{x}\ \sin\alpha_i - \bar{z}\ \cos\alpha_i$$

$$R_{czo} = r_p - 0.5\ d_b\ \cos\alpha_i - \bar{x}\ \sin\alpha_o + \bar{z}\ \cos\alpha_o$$

The z coordinate of this point can be calculated by the following equation:

$$\bar{z} = R_{deform} - \sqrt{(R^2_{deform} - \bar{x}^2)} \qquad (2\text{-}16)$$

where R_{deform} is the radius of curvature of the contact surface (see Fig.2-2c).

The contact surface is a curved surface. According to Hertzian solution, the radius of the contact surface is the harmonic mean of the curvatures of the two contacting bodies

harmonic mean of the curvatures of the two contacting bodies as

$$\frac{1}{R_{deform}} = \left(\frac{1}{0.5\ d_b} + \frac{1}{f\ d_b} \right) / 2 \qquad (2\text{-}17)$$

where f is the curvature factor of the race (f is defined in Chapter 3).

Since the contact area is a narrow ellipse, the curvature in the rolling direction can be neglected, and only the curvature in the transverse direction has to be considered.

Heat Generation Rate

The heat generation rates in each contact is

$$\dot{H} = \int \mu(u_s)\ q\ u_s\ dA \qquad (2\text{-}18)$$

EHD Traction Coefficient

Typical Traction Curve

The bearing analyst needs to know traction coefficients at various sliding speeds (the sliding speed varies within the contact zone). Since the calculation of the EHD traction coefficient is somewhat complicated, it is necessary to establish the traction-sliding relationship (traction curve) prior to the bearing analysis. A typical traction curve as shown in Fig.2-10 exhibits three different regions. The first region is the linear region where the linear relationship of Newtonian flow applies. The second region is the nonlinear

to the non-Newtonian effect. The third region is the thermal region where the traction coefficient falls as the sliding increases.

Parameters in the Traction Curve

The traction curve in the Fig.2-10 can be represented by four parameters: u_m, the sliding speed at which maximum friction occurs; μ_0, the coefficient of friction at zero sliding; μ_m, the maximum coefficient of friction; μ_f, the coefficient of friction at high sliding speeds. In the later analysis of this paper, this traction curve as well as these parameters will be referred to.

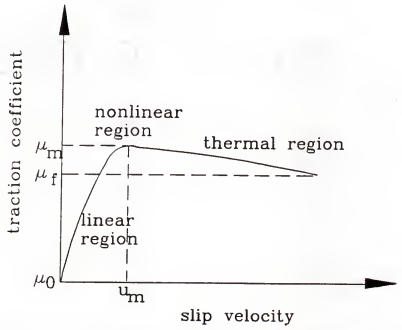

Figure 2-10 Typical traction coefficient of elastohydrodynamic lubrication.

Common Values of Coefficient of Friction

For bearing analysis, the selection of the traction coefficient can make use of Table 2-1 which shows typical values of coefficient of friction for metal-to-metal contacts under various lubrication conditions.

Table 2-1 Typical values of coefficient of friction

type of lubrication	coefficient of friction
lubricated by HD film	0.005-0.02
lubricated by EHD film	0.02-0.1
boundary lubrication	0.08-0.14
dry	0.25-0.4

CHAPTER 3
BEARING GEOMETRIC MODEL AND NUMERICAL PROCEDURE

In bearing analysis, the calculation of contact loads, contact angles, and contact areas requires a complex ball-race interaction model. This chapter presents such a model along with the complete numerical procedure for bearing analysis.

Ball-Race Interaction

Based on Harris' model [1,2], this section develops necessary equations for calculating the interaction caused by preloads, axial loads, radial loads, and tilting moments.

Basic Geometry of Angular Contact Ball Bearing

Some basic bearing geometric parameters are introduced here. Fig.3-1a shows a load-free angular contact ball bearing and the following parameters:

α : contact angle

$f_i\ d_b$: length of the inner race curvature radius

$f_o\ d_b$: length of the outer race curvature radius

The two radii of curvature are slightly larger than the ball radius to ensure point contacts between the balls and races. The contact angle is the angle between the contact line (line connecting the contact point and the ball center) and

the R-axis. Furthermore, in Fig.3-1a, b, and c, Points O', B, and I are called outer race curvature center, ball center, and inner race curvature center, respectively (Fig.3-1b shows a loaded ball bearing). These three centers are often referred to in the later discussion. Also shown in Fig.3-1a, d_{io} is the distance between the two race curvature centers under the load-free condition. This distance is

$$d_{io} = (f_i + f_o - 1)\, d_b$$

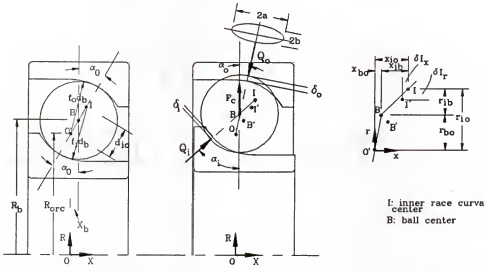

a) an undeformed ball

b) a deformed ball

I: inner race curvature center
B: ball center

c) relative positions of I and B to outer race curvature center O'

Figure 3-1 Notations for the calculation of contact angles and deflections of a ball: a) an unloaded ball; b) a loaded ball; and c) relative positions of Points I and B to O'.

Displacement of the Inner Race

Fig.3-2 shows how a bearing inner race (the big circle) responds to a radial load and a tilting moment. The following

discussion is to determine the displacement of the inner race - in terms of the displacement of the curvature center I of a ball located at the position ϕ_b.

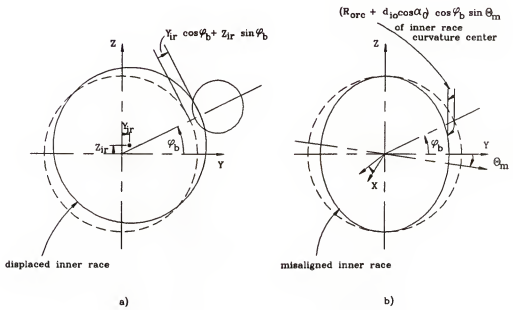

Figure 3-2 Displacement of the inner race (the big circle) due to a) a translation in the Y-Z plane; b) a misalignment angle ($-\theta_m$) about the z-axis.

Some more parameters have to defined, and they are

(X_b, R_b, ϕ_b): the coordinates of the ball center B.

$(0, R_{orc}, \phi_b)$: the coordinates of the outer race curvature center O', and where

$$R_{orc} = r_p - (f_o - 0.5)\, d_b \cos\alpha_0$$

δ_{px}: the displacement of inner race due to axial preload.

δ_{pr}: the displacement of inner race due to radial preload.

(X_{ir}, Y_{ir}, Z_{ir}): the new position of the inner race center when the inner race is subject to a radial load.

Therefore, the displacement of the inner race center I, as represented by δI_x and δI_r, under all possible loads can be rewritten as

$$\delta I_x = \delta_{px} + X_{ir} + (R_{orc} + d_{io} \cos\alpha_0) \cos\phi_b \sin\theta_m$$

$$\delta I_r = (\delta_{pr} + Y_{ir} \cos\phi_b + Z_{ir} \sin\phi_b) \cos\theta_m$$

If there is no tilting moment, the tilting angle θ_m is zero and the above equations become

$$\delta I_x = \delta_{px} + X_{ir}$$

$$\delta I_r = \delta_{pr} + Y_{ir} \cos\phi_b + Z_{ir} \sin\phi_b$$

Deformation Force in the Ball-Race Contact

After the displacements of the inner race center I, δI_x and δI_r, are determined, the equations for calculating the interactions between a ball at position (X_b, R_b, ϕ_b) and the two races are developed here. Again, some new notation is used (referring to Fig.3-1c):

$$x_{ib} = d_{io} \sin\alpha_0 + \delta I_x - (X_b - X_{orc})$$

$$r_{ib} = d_{io} \cos\alpha_0 + \delta I_r - (R_b - R_{orc})$$

$$x_{bo} = X_b$$

$$r_{bo} = R_b - R_{orc}$$

The deflections in the ball/race contact and the contact angles then can be calculated as follows:

For inner race,

$$\alpha_i = \tan^{-1}(x_{ib}/r_{ib}) \tag{3-1a}$$

$$\delta_i = (x_{ib}^2 + r_{ib}^2)^{1/2} - (f_i - 0.5)\, d_b \tag{3-1b}$$

For outer race,

$$\alpha_o = \tan^{-1}(x_{bo}/r_{bo}) \tag{3-1c}$$

$$\delta_o = (x_{bo}^2 + z_{bo}^2)^{1/2}2 - (f_o - 0.5)\, d_b \tag{3-1d}$$

The elastic deformation forces corresponding to the above deflections are

$$Q = K\, \delta^{3/2} \tag{3-2}$$

The ball-race contact stiffness K is dependent on the conformity of the two contacting bodies, and the formula for calculating this stiffness is discussed in Appendix A.

Numerical Procedure for Load Distribution Analysis

The load on each ball in a bearing can be obtained by solving the force equilibrium equations of Eq.(2-5) and (2-8). The variables to be solved are X_{ir}, Y_{ir}, Z_{ir}, X_b, and R_b. The force equilibrium equations are non-linear algebraic equations, therefore, these equations are solved by Newton-Raphson's iteration method in this paper.

Also in the calculation, the balls are assumed to have no effect on each other so that the computation effort can be significantly reduced.

Equilibrium Equations for Paired Angular Contact Ball Bearings

Since angular contact ball bearings are usually mounted in pairs, the force equilibrium equation of Eq.(2-8a) has to include the load caused by the other bearing. The method used here is to add the axial force caused by the other bearing to the external force term in Eq.(2-8a). This method can be expressed as

$$F_x = F_x' + F_{xp}$$

where F_x' is the external force applied to the bearing,

F_{xp} is the axial force caused by the other bearing.

For a pair of angular contact ball bearings preloaded against each other, the centrifugal force will increase the preload between them.

Procedure of Quasi-Static Load Distribution Analysis:

Step 1: Input bearing geometric data, material properties (elastic modulus, density), bearing preload, radial load, and bearing speed.

Step 2: Calculate the centrifugal force by using the free contact angle, and also assume no gyroscopic moment effect (assume the coefficient of friction is zero).

Step 3: Let X_{ir}, Y_{ir}, and Z_{ir} equal zero, .

Step 4: For each ball, assume initial values for X_b and R_b and compute Q_i and Q_o in Eq.(2-5a) and (2-5b).

If Eq.(2-5a) and (2-5b) are satisfied for each ball, go to the next step.

If either Eq.(2-5a) or (2-5b) is not satisfied, using Newton-Raphson's method to obtain new X_b and R_b and repeat this step.

Step 5: Take into account the gyroscopic moment effect. Use calculated Q_i and Q_o for each ball to determine the coefficient of friction by Eq.(2-8c). Repeat Step 4 once again with this coefficient of friction value.

Step 6: Calculate resultant bearing forces F_x, F_y, and F_z by Eq.(2-8a), (2-8b) and (2-8c) (neglecting the friction forces in these equations).

If X_{ir}, Y_{ir}, and Z_{ir} are zero, the value of F_x is stored as F_{xp} to account for the force caused by the other bearing.

If Eq.(2-8a to c) are satisfied, go to next step.

If any of Eq.(2-8a to c) are not satisfied, use Newton-Raphson's method to obtain new X_{ir}, Y_{ir}, Z_{ir} and repeat from Step 4.

Derivatives for the Newton-Raphson's Method

In solving the equilibrium conditions by the Newton-Raphson's method, the derivatives of contact loads and contact angles relative to the ball position are needed. In the following, the derivatives for the inner race contact are

presented. The derivatives for the outer race contact are similar.

$$Q_i/\ X_b = -\ 1.5\ K_{br}\ \delta_i^{1/2}\ x_{ib}/(x_{ib}^2 + r_{ib}^2)^{1/2}$$

$$Q_i/\ R_b = -\ 1.5\ K_{br}\ \delta_i^{1/2}\ r_{ib}/(x_{ib}^2 + r_{ib}^2)^{1/2}$$

$$\alpha_i/\ X_b = x_{ib}/(x_{ib}^2 + r_{ib}^2)$$

$$\alpha_i/\ R_b = -\ z_{ib}/(x_{ib}^2 + r_{ib}^2)$$

Procedure for the Complete Bearing Dynamic Analysis

Time Simulation Procedure

The time-simulation method solves the equations of motion by continuously integrating these equations over a small time step. Time simulation often starts from the initial conditions provided by the race-control theory solution. The integration can be performed by the Runge-Kutta fourth order formulas.

A flow chart of the complete bearing analysis (including load distribution analysis and dynamic analysis) is presented in the next page.

Quasi-Static Analysis

The quasi-static method neglects the inertial force terms $-\ m_b\ R_b\ \ddot{\phi}_b$, $J_b\ \dot{\omega}_x$, $J_b\ \dot{\omega}_y$, and $J_b\ \dot{\omega}_z$ - in the equations of motion, Eq.(2-14a to d). The following iterative procedure is used for this analysis:

1. Fix the loads and contact angles of each ball.

2. Perform a time simulation on each ball until a steady state is reached.

The justification of this procedure is that if the loads and contact angles of a ball are constant, the time simulation will eventually reach a steady state.

Figure 3-3 The flow chart of the time-simulation analysis (including the load distribution analysis and kinematic analysis by the race-control theory.

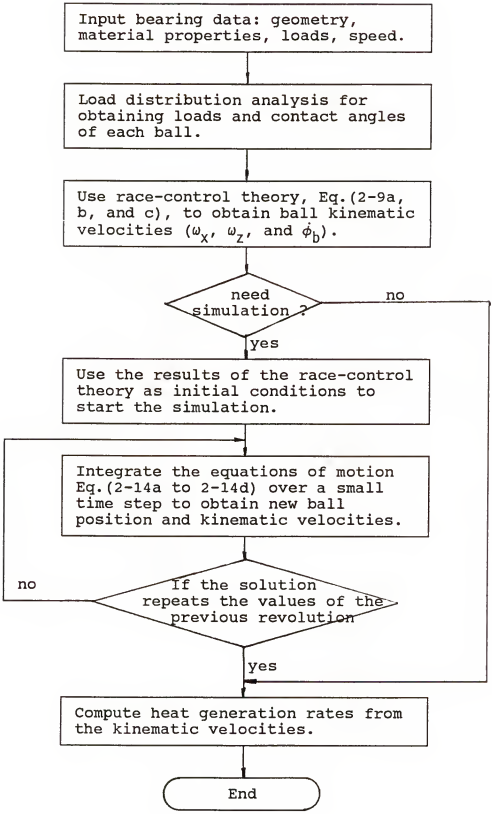
Input bearing data: geometry, material properties, loads, speed.
Load distribution analysis for obtaining loads and contact angles of each ball.
Use race-control theory, Eq.(2-9a, b, and c), to obtain ball kinematic velocities (ω_x, ω_z, and ϕ_b).
need simulation ?
no
yes
Use the results of the race-control theory as initial conditions to start the simulation.
Integrate the equations of motion Eq.(2-14a to 2-14d) over a small time step to obtain new ball position and kinematic velocities.
no
If the solution repeats the values of the previous revolution
yes
Compute heat generation rates from the kinematic velocities.
End

CHAPTER 4
TEMPERATURE DISTRIBUTION AND TRACTION WITHIN ELASTOHYDRODYNAMIC FILMS

As discussed earlier, the traction coefficient between balls and races has a significant influence on the ball motion. This chapter discusses the procedure for calculating the traction coefficient of EHD films. There are three sections in this chapter. Since lubricant viscosity is dependent on temperature, equations for a fast computation of the temperature in the EHD film are derived in the first section. The film thickness formulas and the effects of sliding on the EHD film are discussed in the second section. The third section presents lubricant rheological models and a flow chart for the calculation of traction coefficient.

Bearing Bulk Temperature and Temperature in the EHD Film

Bearing Bulk Temperature

The most important aspect of the bearing bulk temperature is that it determines the EHD inlet temperature and consequently the film thickness. However, the calculation of the bearing bulk temperature is difficult because the heat transfer coefficients required for such calculation are usually unknown. The following equation is written for an

estimation of this temperature. This equation assumes that all the heat generated in a bearing is taken away by a lubricant flow.

$$T_{bulk} = \frac{\dot{H}}{\rho_{oil}\, C_{oil}\, Q} + T_{oil} \qquad (4\text{-}1)$$

where H is the heat generation rate of the bearing, and Q is the oil flow rate.

Energy Equation

Temperature distribution can be calculated from the energy equation as follows:

$$k \frac{\partial^2 \theta}{\partial z^2} + \eta \left(\frac{\partial u}{\partial z} \right)^2 = \rho\, C \frac{\partial \theta}{\partial t} \qquad (4\text{-}2)$$

In this equation, the two terms on the left-hand-side represent the heat conduction in the z-direction and the heat generated due to shearing of the fluid in the film respectively. The right-hand-side term represents the change in the fluid internal energy.

The specific meaning of the energy equation is that the heat generated in the contact is either conducted to the metal boundaries or convected away by the fluid.

Solid Surface Temperature

The temperature on the solid boundary surface can be

calculated by the following equation developed by Archard [27]:

$$\theta_s(Y) = \frac{1}{\sqrt{\pi\ \rho_s\ c_s\ k_s\ v}} \int_{-b}^{y} \frac{-k\ (\frac{\partial\theta}{\partial z})_{z=0\ \text{or}\ h}}{\sqrt{y - \psi}}\ d\psi \qquad (4\text{-}3)$$

where subscript s represents the solid.

This equation can be derived by the analogy of a heat source moving along a semi-infinite surface [13]. Note that v is the rolling speed.

It also can be assumed that the heat transferred into the solid surface is at a constant rate over the contact area; then the integration in Eq.(4-3) can be carried out to give

$$\theta_s(Y) = \frac{k\ (\frac{\partial\theta}{\partial z})_{z=0\ \text{or}\ h}\ \sqrt{y + b}}{\sqrt{\pi\ \rho_s\ c_s\ k_s\ v}} \qquad (4\text{-}4)$$

Temperature Profile Obtained from the Energy Equation

If shearing takes place in the fluid film, the temperature increase in the film can be determined from the energy equation as

$$(1+E)\ \theta = \frac{-q}{2\ k}\ z^2 + c_1\ z + c_2$$

where q is the specific heat generation rate, and

$$E = \frac{\rho\ c\ v\ z^2}{2\ k\ \Delta y} \qquad (4\text{-}5)$$

E is a factor to calculate the heat convected away.

For the boundary conditions

$$\theta = \theta_s \quad \text{at } z = 0 \text{ and } z = h$$

we find

$$\theta = \frac{q}{2\ k\ (1+E)}\ z\ (h-z) + \theta_s \tag{4-6}$$

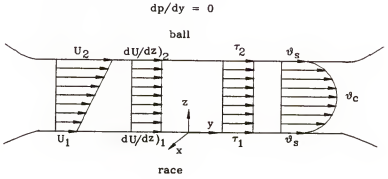

Figure 4-1 Distributions of the velocity, shear rate, stress, and temperature across an EHD film due to sliding.

Shear Stress Distribution (Sliding Occurs)

To calculate the heat generation rate, the shear stress distribution across the film should be determined.

$$\frac{\partial \tau}{\partial z} = \frac{dp}{dy}$$

and according to the boundary condition (Fig.4-1)

$$\tau = \eta \frac{v_{s2}-v_{s1}}{h}, \text{ at } z = \frac{h}{2}$$

Since the shear stress varies linearly along the z-direction, the shear stress due to the pressure gradient is

$$\tau = \frac{dp}{dy}\left(\frac{h}{2} - z\right) + \eta \frac{v_{s2} - v_{s1}}{h}$$

Heat Generation due to Sliding

In the Hertzian contact zone, the heat generation due to the pressure gradient is small. It is reasonable to assume that all the heat is generated from the sliding. In such cases, the strength of the heat source across the film is constant.

If θ_s represents the temperature on the surface and θ_c is the temperature at the center of the film, the following relationship can be written,

$$q = \tau \frac{\partial v}{\partial z} = \text{constant}$$

Thus, when $z = h/2$,

$$\theta = \frac{1}{2k\ (1+E)} \tau \left(\frac{\partial v}{\partial z}\right) z\ (h-z) + \theta_s$$

$$\frac{\partial \theta}{\partial z} = \frac{1}{2k\ (1+E)} \tau \left(\frac{\partial v}{\partial z}\right) (h-2z)$$

for $h = h/2$, and the temperature at the central plane, θ_c can be obtained.

$$\theta_c = \frac{1}{2k\ (1+E)} \tau \left(\frac{\partial v}{\partial z}\right) \frac{h^2}{4} + \theta_s \qquad (4\text{-}7)$$

and now $E = (\rho\ C\ V\ h^2\ /\ 8\ k\ \Delta y)$

For the calculation of θ_s, the heat transferred to the solid boundary is

$$- k \left|\frac{\partial \theta}{\partial z}\right|_{z=0 \text{ or } h} = \frac{1}{2\ (1+E)}\ \tau\ \left(\frac{\partial v}{\partial z}\right)\ h$$

Temperature Increase due to Pressure Gradient (for no Sliding)

Sliding represents the major heat source in a bearing and the temperature rise caused by sliding is much higher than that caused by pure rolling. When there is no sliding, heat generation is due to the pressure gradient and is only significant in the inlet region. The temperature distribution for a no-sliding case is presented here.

By following the similar procedure in the previous section and assuming

$\theta = \theta_s$ at $z = 0$ and $z = h$

then the temperature distribution becomes

$$\theta = \frac{q}{2\ k\ (1+E)}\ (h-z)\ z + \theta_s$$

where q is the specific heat generation which can be determined by

$$\tau = \frac{dp}{dy}\ \left(\frac{h}{2} - z\right)\ \frac{\partial v}{\partial z}$$

since

$$q = \tau \frac{\partial v}{\partial z}$$

we can write

$$q = \frac{1}{2\ k\ \eta} \left[\frac{dp}{dy} \left(\frac{h}{2} - z\right)\right]^2$$

By substituting the above heat generation rate into the temperature distribution, the following relationship can be written,

$$\theta = \frac{1}{2\ k\ \eta\ (1+E)} \left[\frac{dp}{dy} \left(\frac{h}{2} - z\right)\right]^2 z\ (h-z) + \theta_s$$

In order to obtain the location where the maximum temperature is, the temperature is differentiated over z,

$$\frac{\partial \theta}{\partial z} = \frac{1}{(2k)4\eta\ (1+E)} \left(\frac{dp}{dy}\right)^2 \left[(h-2z)(8z^2 - 8zh + h^2)\right]$$

Thus, the maximum temperature occurs at the following positions (as shown in Fig.4-2):

$$z = \frac{2 \pm \sqrt{2}}{4} h$$

$$\theta_{max} = \frac{1}{(2k)4\eta\ (1+E)} \left(\frac{dp}{dy}\right)^2 \frac{1}{16} h^4 \qquad (4\text{-}8)$$

and now $E = ((3-2\sqrt{2})\ \rho\ C\ V/\ 16\ k\ \Delta y)$

For the calculation of θ_s, the heat transferred to the solid boundary is

$$-k \left|\frac{\partial \theta}{\partial z}\right|_{z=0 \text{ or } h} = \frac{1}{(2k)4\eta\ (1+E)} \left(\frac{dp}{dy}\right)^2 h^3$$

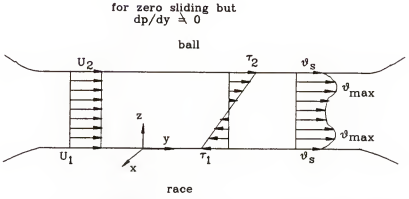

Figure 4-2 Distributions of the velocity, stress, and temperature across an EHD film due to a pressure gradient (sliding is zero).

EHD Film Thickness and Effects of Sliding

This section presents the film thickness formulas and discusses briefly how these formulas are derived. It has been found that sliding has only a modest effect on the film thickness. An explanation of this EHD property is also presented.

The Reynolds Equations

The primary purpose of lubrication is to reduce friction and wear between two rubbing bodies by inserting a low shearing material between them. The lubrication effects of an

elastohydrodynamic film are accomplished by the fluid actions governed by the Reynolds equation (one-dimensional):

$$\frac{\partial}{\partial y}\left(h^3 \frac{\partial p}{\eta\, \partial y} \right) = 12\,(v_1 + v_2)\,\frac{\partial h}{\partial y} \qquad (4\text{-}9)$$

The derivation of the Reynolds equation and the method for solving this equation are presented in Appendix B.

Film Thickness for EHD Lubrication

The most important parameter, the film thickness, can be calculated by using the formulas presented by Hamrock and Dowson. The following film thickness formulas are known as the isothermal film thickness formulas because they are obtained by assuming the viscosity is constant across the z-direction. The minimum film thickness

$$\frac{h_0}{R} = 3.63\,\frac{U^{0.68}\,G^{0.49}\,(1-\,e^{-0.68\kappa})}{W^{0.063}} \qquad (4\text{-}10)$$

The central film thickness,

$$\frac{h_c}{R} = 2.69\,\frac{U^{0.67}\,G^{0.53}\,(1-0.61\,e^{-.73\kappa})}{W^{0.067}} \qquad (4\text{-}11)$$

where G, R, U, W and κ are non-dimensional parameters

G: elastic parameter

R: equivalent radius (defined in Appendix A)

U: speed parameter

W: load parameter

κ: ratio of contact area axes

and,

$$U = \frac{\eta_0 (u_1 + u_2)}{2 E' R}$$

$$W = \frac{Q}{E' R^2}$$

$$G = \alpha E'$$

where η_0 : the inlet viscosity

α : the viscosity-pressure factor (generally, its value is between 0.01 and 0.02 mm^2/N)

Derivation of the Film Thickness Formulas

The film thickness formulas are derived by solving the Reynolds equation, elasticity theory, and lubricant rheology for various sets of values of the EHD parameters (G,R,U,W,κ). The exponent of each parameter is determined by the least-square curve fitting for exponential function.

Film Thickness for Hydrodynamic (HD) Lubrication

It is very difficult to solve the Reynolds equation, but for a simpler case, the HD lubrication, the film thickness can be more or less observed from the integrated Reynolds equation. The integrated Reynolds equation:

$$\frac{\partial p}{\partial y} = 12 \eta V \frac{h - h_m}{h^3} \qquad (4\text{-}12)$$

where h_m is the film thickness at a location where maximum pressure occurs (dp/dy = 0).

It can be found that the above equation is similar to the film thickness formula for HD lubrication:

$$\left(\frac{h}{R}\right)^2 = C \frac{\eta V}{P} \qquad (4\text{-}13)$$

where C is a constant.

By comparing Eq.(4-10) and Eq.(4-13), it can be found that the major difference between the EHD and HD lubrications is that load has a very small effect on the EHD film thickness.

EHD Pressure Profile and Film Shape

The key reason that an EHD film can develop in a highly loaded contact is that the pressure of the fluid flow can create a coherent channel for the fluid flow itself. The EHD lubrication thus has the following two features (referring to Fig.4-3):

First, the film should have a constant thickness over the high pressure area, and the pressure distribution should be similar to the Hertzian pressure distribution. The film thickness has to be constant, i.e., the channel has to be flat, because the viscosity in the contact region is high and a small gradient of the film shape can result in a large

pressure gradient. In order to create a flat film shape, the pressure distribution has to be Hertzian.

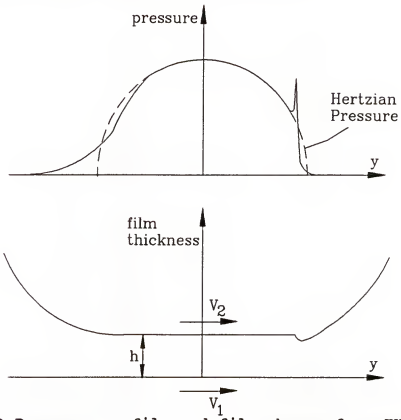

Figure 4-3 Pressure profile and film shape of an EHD film.

Second, there is a pressure spike near the exit and a constriction of the channel immediately following the pressure spike. The pressure spike occurs because the flow in the exit has to satisfy the Reynolds boundary condition which stipulates that sub-ambient pressure (the cause of cavitation) should not occur:

$dp/dy = 0$, at the exit

According to this boundary condition, the pressure profile must fall inside the Hertzian profile in the exit

region. A pressure spike thus occurs to produce two effects: first, it causes the fluid pressure to fall rapidly to meet with the boundary condition; second, it makes up the pressure difference between the fluid pressure profile and the Hertzian profile in the exit region. Again, in order to create a pressure spike, the channel has to be narrowed. The film thickness at the constriction is called the minimum film thickness.

Effects of Sliding on Film Thickness and Pressure Spike

An important property of the EHD film is that sliding has only a moderate effect on the film thickness. This property can be seen from the film thickness formulas.

First, it can be seen that the viscosity used in the film thickness calculation is the inlet viscosity - η_0. This means that although the temperature in the contact region may be high, the film thickness will not be affected by this temperature. This EHD property can be explained by the fact that the deformation of the metal surfaces and the fluid action are mutually dependent, thus change of viscosity in the contact zone only affects the slopes of the film shape but not the thickness. It can further be inferred that an EHD film rarely fails because the inlet temperature is commonly low.

Second, the speed used in the film thickness formulas is called the entraining speed which is the average of the two

surface speeds. Since in rolling bearings the predominant motion is rolling, the sliding contribution is small.

As for the pressure spike, it can also be expected that sliding does not have a significant influence on it. This is because the pressure spike is generated to satisfy the Reynolds boundary condition (to avoid cavitation). Sliding does not change the boundary condition.

Lubricant Deterioration

Because lubricants have relatively low conductivity, high temperatures in the lubricating film are expected. Besides affecting the working viscosity, high temperature may lead to significant chemical reactions (oxidation or polymerization) and lubricant deterioration. It has been pointed out that lubricant deterioration becomes critical when the temperature exceeds 66°C (the rate of oxidation doubles for each 10°C rise in temperature of the oil above 66°C). The chemical reactions can develop increased viscosity, acids, carbon residue, and sludge. However, since lubricant passes through the contacts in a short period of time, lubricant deterioration is not a problem of concern unless only a trace of lubricant is used.

Non-Newtonian Models and Procedure for Calculating EHD Traction Coefficient

The EHD traction behaves as described by the traction curve in Fig.2-10. The calculation of such traction curve requires detailed lubricant rheological data. Since it is

cumbersome to calculate the traction coefficient while solving the equations of motion for a bearing, the traction curve, as suggested by Gupta [3], is better to be determined before performing bearing analysis.

Non-Newtonian Behavior

The Newtonian fluid model as shown below is not applicable in the traction calculation for EHD lubrication:

$$\tau = \eta \frac{u}{h} \tag{4-14}$$

The calculation of traction should use non-Newtonian models as introduced below. The non-Newtonian behavior arises from the fact that the increase of lubricant viscosity causes the lubricant to behave as a solid. A solid may display elastic and plastic behaviors which are the causes of the non-Newtonian behavior. The following is a frequently used non-Newtonian model.

Visco-Elastic Model and Nonlinear Viscous Model

The combined solid and fluid (viscous) behavior can be described by a model which is a combination of the Maxwell visco-elastic model and the nonlinear viscous model. This model states that the total strain rate of the fluid element is the sum of the elastic and viscous strain rates.

$$\dot{\gamma} = \dot{\gamma}_e + \dot{\gamma}_v = \frac{1}{G^*} \frac{d\tau}{dt} + \frac{\tau_1}{\eta} \tanh^{-1} \frac{\tau}{\tau_1} \tag{4-15}$$

where G^* = fluid shear modulus (N/m^2)

G^* = lubricant shear modulus = $E/(2\ (1+\nu))$

$\dot{\gamma}_e$ = elastic stain rate (1/sec)

$\dot{\gamma}_v$ = viscous strain rate (1/sec)

τ_l : the limiting shear stress

The elastic deformation rate in Eq.(4-15) is usually much smaller than the viscous strain rate and can be neglected. Thus, Eq.(4-15) becomes

$$\dot{\gamma} = \frac{\tau_l}{\eta} \tanh^{-1} \frac{\tau}{\tau_l} \qquad (4\text{-}16)$$

It can be noted that the viscous term is treated by a non-linear function since the viscosity of lubricant behaves non-linearly. Ree-Eyring (1955) has proposed a " sinh " function to describe the nonlinear viscous behavior. The " $\tanh^{-1}$ " is a more recent model proposed by Bair and Winer [20].

The limiting shear stress is usually determined from experiments by using the following expression.

$$\tau_l = C\ P - \tau_0 \qquad (4\text{-}17)$$

where P is pressure, and C is a constant which has to be determined from experiments. Eq.(4-17) is a form that is suitable for experiments.

Calculation of Viscosity

Viscosity is a fluid property which is defined as the resistance of fluid to shear motion. Viscosity is very sensitive to pressure and temperature. There are two models which can be used to determine the lubricant viscosity. The first model is proposed by Barus as follows:

$$\eta(p,\theta) = \eta_0 \exp[\alpha p+\beta(\theta_0-\theta)] \qquad (4\text{-}18)$$

where η_0 is the dynamic viscosity at atmospheric pressure, α is the viscosity-pressure factor, β is the viscosity-temperature factor, and θ_0 is a reference temperature.

Due to the fact that the Barus formula gives extremely high viscosity at high pressures, another equation has been proposed by Roelands, who used his physical-chemical background to obtain (1966)

$$\frac{\log_{10}(\eta) + 1.2}{\log_{10}(\eta_0) + 1.2} = \left(\frac{\theta_0 + 135}{\theta + 135}\right)^{S_0} \left(1 + \frac{p}{2000}\right)^{Z_1} \qquad (4\text{-}19)$$

The non-dimensional parameters Z_1 and S_0 can be calculated from the coefficients α and β in the Barus formula.

$$Z_1 = \frac{\alpha}{5.1 \times 10^{-9} \left(\ln(\eta_0) + 9.67 \right)} \qquad (4\text{-}20)$$

$$S_0 = \frac{\beta \, (\theta_0 + 135)}{\left(\ln(\eta_0) + 9.67 \right)} \qquad (4\text{-}21)$$

After some manipulations, the Roelands viscosity can be expressed as

$$\eta = \eta_0 \exp([\ln(\eta_0)+9.67] [-1+ (1+5.1 \times 10^{-9} p)^{z1} (\frac{\theta +135}{\theta_0+135})^{-S0}])$$

(4-22)

Experimental Data for SAE 30 Motor Oil

Viscosities of SAE 30 Motor oil under various conditions (measured by the falling ball viscometer [25]) are listed in Table 4-1. The reference condition is chosen as 40°C and 1 atm, the reference viscosity is

$\eta_0 = 0.071$ Pa•sec

The values of α and β can be obtained by interpolating the experimental data in relation to the Barus formula, and the results are

$\alpha = 1.5 \times 10^{-8}$ (1/Pa)

$\beta = 0.008$ (1/°C)

Comparison Between the Barus Formulas and the Roelands Formula

The parameters in the Roelands formula can also be determined as

$z_1 = 0.42$

$S_0 = 0.2$

Viscosity values under different pressures calculated by Barus and Roelands formulas for the temperature at 40°C are listed as in Table 4-2. The Roelands formula is an improved

formula which is considered to be more accurate. It can be seen that the results of Barus formula are unreasonably high.

Table 4-1 Measured viscosity data for SAE 30 motor oil [25].

viscosity (10^{-3} Pa·sec)	temperature (°C)		
pressure (MPa)	40	100	150
Atm.	71.0	8.98	3.07
34.5	144.0	15.4	5.35
69.0	291.0	27.2	8.29
138.0	1222.0	65.4	17.1
207.0	3766.0	-	-
276.0	10817.0	325.0	57.2
345.0	-	-	-
414.0	-	1144.0	185.0
524.0	-	-	366.0
552.0	-	6130.	-

Table 4-2 A comparison between the calculated viscosity values from the Barus formula and Roelands formula.

pressure (N/m^2)	η (Barus)	η (Roelands)
0.5×10^9	$1808\ \eta_0$	$139\ \eta_0$
1×10^9	$3.36 \times 10^6\ \eta_0$	$2947\ \eta_0$
2×10^9	$1.07 \times 10^{13}\ \eta_0$	$92900\ \eta_0$

Procedure for Calculating Traction Coefficient

The procedure of calculating traction coefficient is outlined in Fig.4-3.

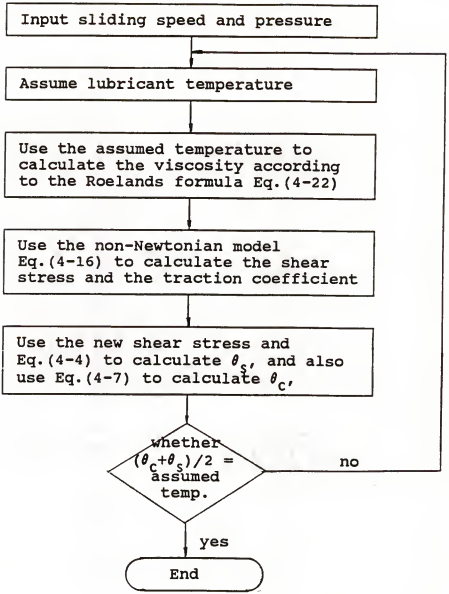

Figure 4-4 The flow chart for calculating traction coefficients.

CHAPTER 5
BEARINGS UNDER INVESTIGATION

Bearing Dimensions and Catastrophic Failure

Bearing Dimensions

The bearings investigated in this work are two bearings used on two different milling spindles. The major difference between these two bearings is in their contact angles - one is 15°, and the other is 60°. Throughout this paper, the following designations are used:

Bearing A: a 15° contact angle ball bearing, 90 mm bore.
Bearing B: a 60° contact angle ball bearing, 90 mm bore.

Bearing internal geometry varies from company to company, thus for reasons of comparison, it is justified to assume that the two bearings have the same internal geometry except for the contact angle (in fact, contact angle is the most important factor affecting heat generation). The following are the data for these bearings which data are typical for bearings of 7018 series (90mm bore).

ball diameter D_b = 12 mm

inner race curvature factor f_i = 0.52

outer race curvature factor $f_o = 0.52$

pitch diameter $d_p = 115$ mm

bore diameter = 90 mm

no. of ball = 20

ball density = 7800 kg/m^3 (steel)

ball mass $m_b = 0.007$ kg

ball inertia $J_b = 1.02 \times 10^{-7}$ kg-m^2

bearing material(steel) $E = 2.08 \times 10^5$ N/mm^2

Poisson's ratio = 0.3

Catastrophic Failure of Bearing B

When the speed of Bearing B reached 9,300 rpm in a test run, it failed suddenly; below that speed, this bearing ran stably. This bearing is a double row bearing, and the failure only occurred in one row - the less lubricated row (this bearing is mounted on a vertical spindle, thus more flow goes into the lower row than into the upper row). Fig.5-1a is a photograph of the undamaged row, and Fig.5-1b shows the damaged row. It can be seen that craters were formed on some of the balls in the failed row. This indicates that the bearing temperature reached a very high level.

Bearing-Spindle Systems and Bearing Bulk Temperature

This section shows the configurations of the spindles which contain the two bearings to be investigated. These two spindles have been run continuously at 6,000 rpm for at

a)

b)

Figure 5-1 Photographs of the angular contact ball bearing in Spindle 1: a) the undamaged row (due to better lubrication); b) the damaged row, craters on ball can be seen on the top several balls. Failure occurred when this bearing was accelerated to 9,300 rpm.

least an hour. The operating temperatures on the outer races of these two bearings have been recorded.

Bearing A and Spindle 1

This spindle consists of five 15° contact angle ball bearings (Bearing A represents the three bearings on the tool end) as shown in Fig.5-2. Small contact bearings allow the spindle to operate at high speeds. Since 15° contact angle bearings have relatively low axial stiffness, a large number of bearings (5 bearings) are used.

After running at 6,000 rpm for one hour, the temperature rise on the outer race was 10°C. The bearings were lubricated by grease.

Bearing B and Spindle 2

Bearing B (60° contact angle) is used in Spindle 2 to support axial loads. This spindle is equipped with two cylindrical roller bearings which provide substantial radial stiffness (see Fig.5-3).

After running at 6,000 rpm for an hour, the temperature rise on the outer race was 20°C. This bearing was lubricated by circulating oil flow.

Calculation of the Hertzian Parameters

The equivalent radii and Hertzian parameters (a*, b*, and δ*) which are needed for the load distribution analysis are calculated in this section using the prescribed bearing

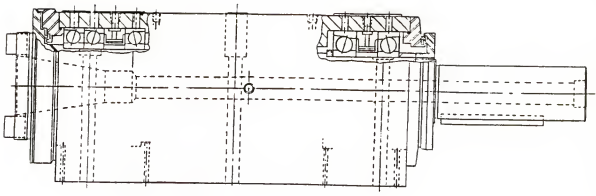

Figure 5-2 Spindle 1, consisting of five 15° contact angle ball bearings.

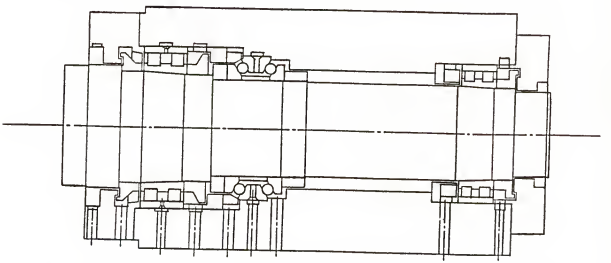

Figure 5-3 Spindle 2, consisting of two cylindrical roller bearings and a 60° contact angle, double row ball bearing.

geometry data and related equations in Appendix A. This section only shows the calculation for Bearing A.

Calculation of the Hertzian Parameters

For inner race,

$r_{bx} = 0.5\ D_b = 6$ mm, $\quad r_{by} = 0.5\ D_b = 6$ mm

$r_{rx} = -\ f_i\ D_b = -\ 6.24$ mm, $\quad r_{ry} = (d_p - D_b \cos\alpha_0)/2 = 51.7$ mm

$$\frac{1}{R_x} = \frac{1}{r_{bx}} + \frac{1}{r_{rx}} = \frac{1}{6} + \frac{-1}{6.24} = \frac{1}{156} \quad \text{mm}^{-1}$$

$$\frac{1}{R_y} = \frac{1}{r_{by}} + \frac{1}{r_{ry}} = \frac{1}{6} + \frac{1}{51.7} = \frac{1}{5.376} \quad \text{mm}^{-1}$$

$$\frac{1}{R} = \frac{1}{R_x} + \frac{1}{R_y} = \frac{1}{156} + \frac{1}{5.376} = \frac{1}{5.197} \quad \text{mm}^{-1}$$

Making use of the Eq.(A-17a to c), we obtain,

$$\kappa = 1.0339 \left(\frac{R_x}{R_y}\right)^{0.6360} = 8.8051$$

$$E_1 = 1.5277 + 0.6023 \ln(R_x / R_y) = 3.556$$

$$E_2 = 1.0003 + \frac{0.5968}{(R_x/R_y)} = 1.0209$$

$$a^* = \left(\frac{2\ \kappa^2\ E_2}{\pi}\right)^{1/3} = 3.6935$$

$$b^* = \left(\frac{2\ E_2}{\pi\ \kappa}\right)^{1/3} = 0.4195$$

$$\delta^* = \frac{2\ E_1}{\pi}\ (\frac{\pi}{2\ \kappa^2\ E_1})^{1/3} = 0.6129$$

for outer race

$r_{bx} = 0.5\ D_b = 6$ mm, $r_{by} = 0.5\ D_b = 6$ mm

$r_{rx} = -f_o\ D_b = -6.24$ mm, $r_{ry} = -(d_p + D_b \cos\alpha_0)/2 = -63.3$ mm

thus,

$R_x = 156$ mm , $R_y = 6.625$ mm , $R = 5.170$

Similarly, the following Hertzian parameters can be obtained:

$\kappa = 7.7096$, $E_1 = 3.4304$, $E_2 = 1.0256$

$a^* = 3.3856$, $b^* = 0.4391$, $\delta^* = 0.6450$

Including the Material Data into Hertzian Formulas

The material properties can be incorporated into the Hertzian formulas, Eq.(A-8), (A-9), and (A-10). If the material is steel,

$E = 2.08 \times 10^{11}$ N/m^2, $\nu = 0.3$

and

$$E' = \frac{E}{1 - \nu^2} = 2.28 \times 10^{11}\ \text{N/m}^2$$

The Hertzian formulas become

$$K_{br} = 2.14 \times 10^5\ \delta^{*-3/2}\ R^{1/2}$$

$$a = 0.0236\ a^*\ (Q\ R)^{1/3}$$

$$b = 0.0236\ b^*\ (Q\ R)^{1/3}$$

CHAPTER 6
RESULTS AND DISCUSSION

It should be recalled here that the two bearings under investigation are (discussed in Chapter 5)

Bearing A: free contact angle $\alpha_0 = 15°$

Bearing B: free contact angle $\alpha_0 = 60°$

The friction in the ball-race contact is assumed to obey the traction curve as illustrated in Fig.2-3. Based on available experimental data [10,11,12], the parameters in the traction curve are assumed to be (two other traction curves will be assumed later)

Traction Curve 1:

$u_m = 0.2$ m/sec

$\mu_0 = 0$

$\mu_m = 0.054$

$\mu_f = 0.054$

It can be seen that this traction curve assumes traction coefficient levels off at high sliding speeds.

The analysis includes four steps. First, the loads and contact angles of each ball are calculated. Second, the race-control theory is used to compute the ball spinning friction

and the heat generation over a range of the speed. Third, the time-simulation method is used to investigate the ball skidding phenomenon caused by the gyroscopic moment effect. Lastly, the lubrication film thickness and temperature distribution are calculated.

Load Distribution

The loads, the contact angles, and the contact areas of each ball have to be determined by solving the force equilibrium equations, Eq.(2-4). This section shows calculated results for one particular case for each bearing.

For Bearing A at 10,000 RPM

For the prescribed loading conditions, the calculated results are listed as follows:

axial preload : 1,000 N

bearing speed : 10,000 rpm

operating contact angles:

$\alpha_i = 21.06°$, $\alpha_o = 13.96°$

loads:

$Q_i = 163.7$ N , $Q_o = 251.6$ N

contact areas:

for inner race

a = 0.8259 mm , b = 0.0938 mm

and for outer race,

a = 0.8722 mm , b = 0.1131 mm

For Bearing B at 9,500 rpm

For the operating conditions:

axial preload : 1,000 N

bearing speed : 9,500 rpm

operating contact angles:

$\alpha_i = 68.73°$, $\alpha_o = 51.70°$

loads:

$Q_i = 247.5$ N , $Q_o = 300.9$ N

contact areas:

for inner race

a = 0.9427 mm , b = 0.1111 mm

and for outer race,

a = 0.9955 mm , b = 0.1252 mm

General Ball Motion Based on the Race-Control Theory

The race-control theory provides a convenient method to compute the bearing kinematics when the gyroscopic moment is small. In this section, the controlling race is assumed to be the outer race. The heat generation rates resulting from ball spinning are also calculated.

The rolling, spinning (only on the inner race), and the spin-to-roll ratio for Bearing A and Bearing B are shown in Fig.6-1 and Fig.6-2. Due to the centrifugal force, the spin-to-roll ratios increase as the speed increases. The heat generation rates are shown in Fig.6-3.

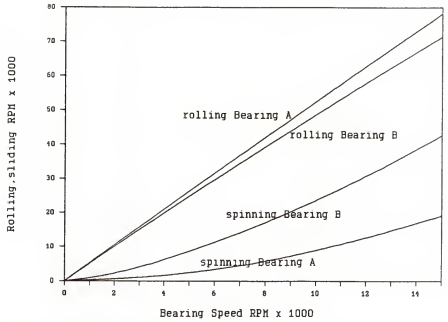

Figure 6-1 Spinning and rolling velocities in Bearing A (15° contact angle) and Bearing B (60° contact angle), both bearings are preloaded by 1000 N.

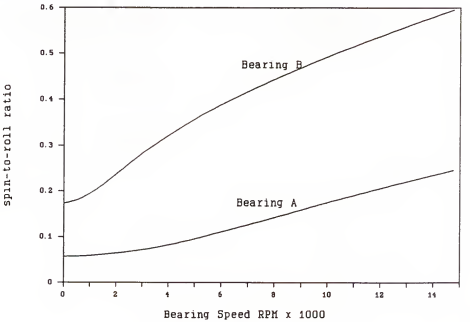

Figure 6-2 Spin-to-roll ratios for the two bearings under 1000 N preload.

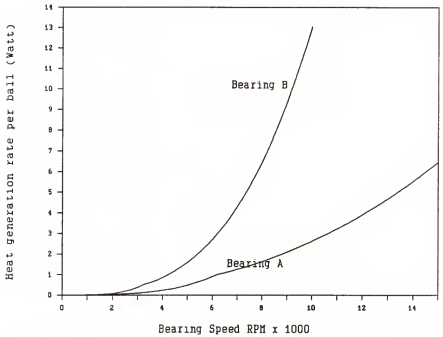

Figure 6-3 Heat generation rates due to ball spinning of the two bearings under 1000 N preload.

Time-Simulation Solution for Ball Skidding Motion

As mentioned, Bearing B represents a bearing which failed at 9,300 rpm in a test run. A time simulation is performed to investigate the ball motion and heat generation rate in the 9,300 rpm neighborhood.

Using Race-Control Theory to Determine the Threshold Speed of Ball Skidding

To determine the threshold speed of ball skidding, the gyroscopic moment, $J_b \dot{\phi}_b \omega_z$, and the resistant torque, $\mu Q d_b$, in the minimum preload condition are calculated for a range of speeds based on the race-control theory. The minimum preload condition:

$$J_b \dot{\phi}_b \omega_z < \mu Q d_b \qquad (2\text{-}7)$$

For Bearing A, the results in Fig.6-4 indicate that the gyroscopic moment is always smaller than the resistant torque. The results for the Bearing B in Fig.6-5 indicate that the gyroscopic moment exceeds the frictional torque at about 9,000 rpm, and this means that the ball skidding is expected to occur at this speed.

Speeds for Time Simulations

In order to understand the ball motion at the speeds around 9,000 rpm, time simulations are performed for the following three speeds:

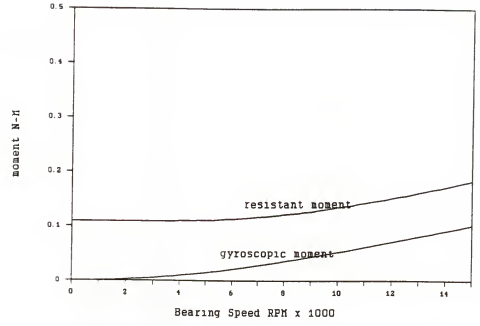

Figure 6-4 Gyroscopic moment and the resistant moment on Bearing A (15° contact angle) under 1,000 N preload.

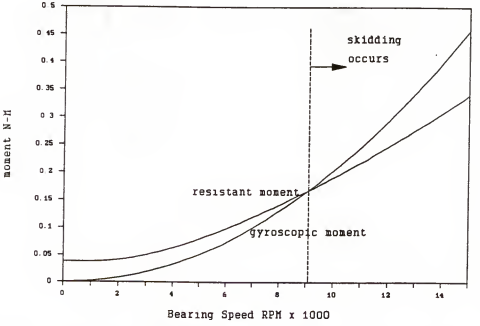

Figure 6-5 Gyroscopic moment and the resistant moment on Bearing B (60° contact angle) under 1,000 N preload.

7,500 rpm

8,500 rpm

9,500 rpm

If there is no radial load, the time-simulation method and quasi-static method are virtually the same method.

Format of the Time-Simulation Output Plots

The time-simulation outputs are plotted in a form that can be found in Fig.6-6. The following features of these plots should be noted.

1. The horizontal axis shows the ball position which is used in place of time (ball position is proportional to time). Note that the balls are circulating inside the bearing.
2. The initial conditions, the values at the vertical axis, are data from the race-control theory.
3. The initial part of each plot showing a transient variation should be ignored.

Time-Simulation Results for no Radial Load Conditions

Fig.6-6 shows that the heat generation rate almost doubles (from 32 Watts to 57 Watts per ball) when the speed increases from 8,500 to 9,500 rpm. This is a significant increase of heat generation and is believed to be the cause of the failure of Bearing B. It also can be seen that the heat generation rate calculated from the time simulation is five times that calculated from the race-control theory.

The time simulation also shows that the gyroscopic moment already increases the heat generation rate at 7,500 rpm which is lower than the speed predicted by the race-control theory. This is because the ball spinning is occurring at the same time.

When the ball skidding occurs, the ball motion represented by the four velocity components - ω_x, ω_y, ω_z, and $\dot{\phi}_b$ - is shown in Fig.6-7. The most important point of this figure is that ω_y which represents the skidding speed is not zero. Furthermore, since other velocity components also depart from the solutions given by race-control theory (which implies no gross sliding), gross sliding is clearly seen to be present in this bearing.

The difference between the heat generation rates calculated by the time-simulation method and the race-control theory is shown in Fig.6-8. This figure shows that ball skidding causes substantial increase of heat generation. It also can be found that the ball spinning friction in Bearing B is already higher than that of Bearing A.

Time Simulation for Bearing B Under a Radial Load

If a radial load is present, the load distribution on the Bearing B is non-axisymmetrical, and the rotational speeds of each ball undergo a time-cycle variation.

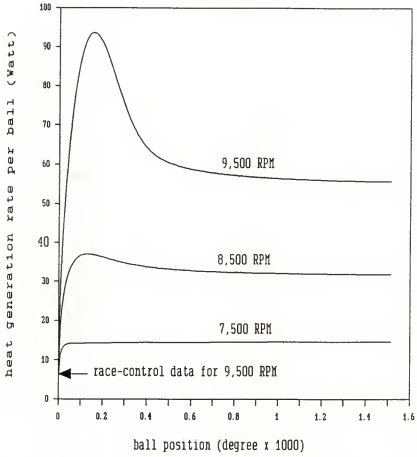

Figure 6-6 Heat generation of Bearing B for different speeds (for axisymmetrical loading, the time-simulation and quasi-static method results are the same). The initial values are the race-control theory results, and the initial transient variation should be ignored.

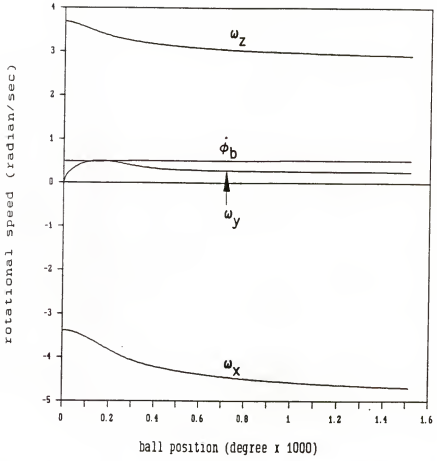

Figure 6-7 Time simulation solutions for ball rotational speeds. The shaft speed is 9,500 RPM. The initial values are race-control theory results, and the initial transient variation should be ignored.

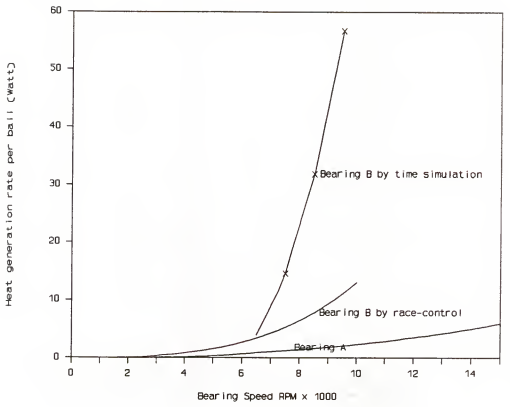

Figure 6-8 Heat generation rates calculated by the race-control theory and time simulation method. Both bearings are under 1000 N axial preload. (For Bearing A the time simulation results are close to the race-control theory results)

Load distribution in a radially loaded bearing. Fig.6-9 and Fig.6-10 show the loads and contact angles of each ball. The operating condition is: 1000 N axial preload, 500 N radial load, and 9500 rpm. If the radial load is not present, the loads and contact angles are

Q_i = 247.5 N, Q_o = 300.9 N, α_i = 68.73°, α_o = 51.70°

Heat generation in a radial loaded bearing. The heat generation in this bearing is shown in Fig.6-11. An enlarged section of Fig.6-11 is shown in Fig.6-12. It can be seen that the time simulation has been performed for five revolutions of the balls. The peaks of the time-simulated curve correspond to the lowest loaded position, and the valleys to the highest loaded position.

Fig.6-11 shows that a radial load can significantly increase the magnitude of the ball skidding. The maximum heat generation rate reaches 100 Watts (at the final state) which is twice the heat generated in the pure axial load case.

The heat generation in a ball results from three sources: lateral sliding and slidings in the rolling direction at the inner and outer races. This is the reason why the heat generation per ball does not varies smoothly with the position of ball (as shown in Fig.6-13).

Comparison between the quasi-static solution and the time-simulation solution. In Fig.6-11 and 6-12, the quasi-static solution is represented by the curve marked with the

"+" symbol (each symbol represents a ball). It can be easily seen that the quasi-static results are much smaller than the time-simulation results. Fig.6-14a and b provide an explanation. The quasi-static solution is obtained by calculating the equilibrium conditions for each ball at different positions and does not consider the "history" of ball motion. However, sometimes (as in this case) the friction torque between balls and races is not enough to change the ball spinning axis, and in such a situation, the variation of the direction of the ball spinning axis deviates from the quasi-static solution.

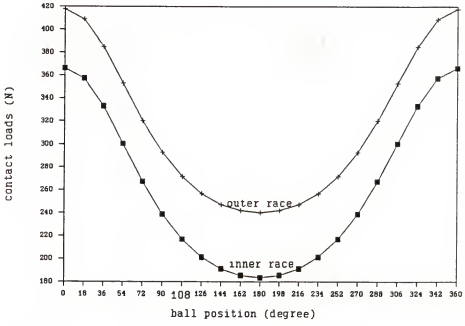

Figure 6-9 Load distribution on each ball in Bearing B (500 N radial load, 1000 N preload, and 9,500 RPM). If there is no radial load, Q_i = 247.5 N and Q_o = 300.9 N.

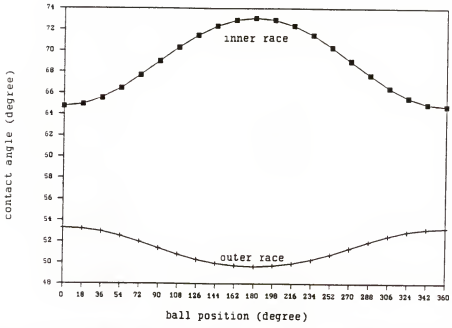

Figure 6-10 Contact angles of each ball in Bearing B (500 N radial load, 1000 N preload, and 9,500 RPM). If there is no radial load, α_i = 68.73° and α_o = 51.70°.

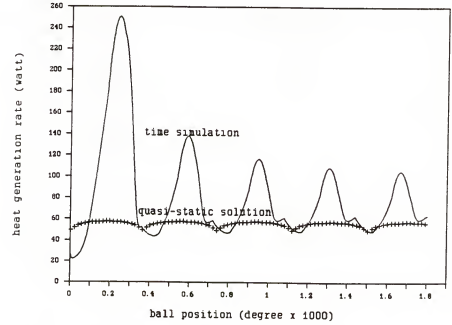

Figure 6-11 Heat generation in Bearing B when it is under a radial load (the time simulation and quasi-static methods show different results).

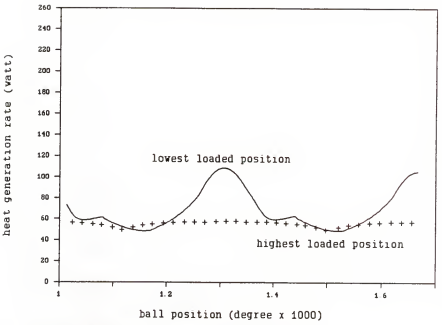

Figure 6-12 An enlarged section of Fig.6-11.

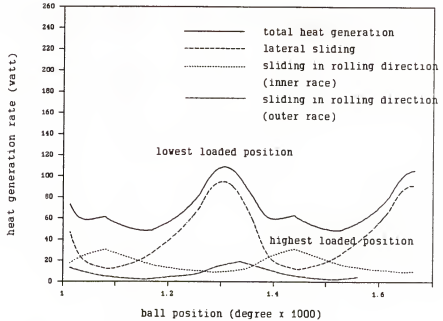

Figure 6-13 Heat generation in a ball results from three sources: lateral sliding and slidings in the rolling direction at the inner race and outer race.

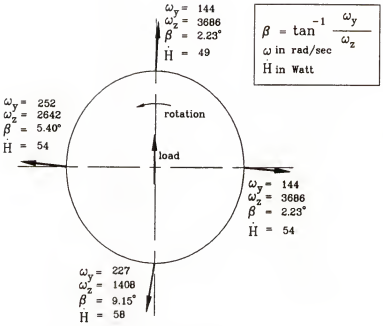

a) quasi-static solution

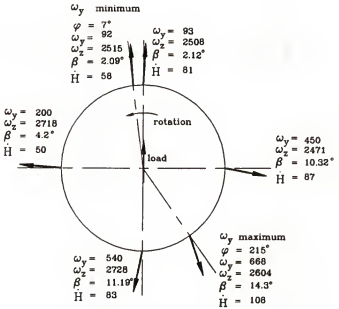

b) time simulation solution

Figure 6-14 Heat generation for a ball at different positions (for Bearing B): a) is calculated by the quasi-static method and b) is calculated by the time simulation method.

Temperature Distribution in the EHD Film

The temperature distribution in the EHD contacts is calculated in this section. The main purpose of calculating temperature distribution is to determine the traction coefficient.

Elastohydrodynamic Film Thickness

In order to calculate the temperature distribution, the elastohydrodynamic film thickness has to be computed first. The following lubricant properties are used for this computation:

η (absolute viscosity at atmosphere condition) = 0.08 Pa·sec

α (viscosity-pressure factor) = 2.0×10^{-8} (1/Pa)

The Hamrock-Dowson central film thickness formula is used:

$$\frac{h_c}{R} = 2.69 \frac{U^{0.67} G^{0.53} (1-0.61\, e^{-0.73\kappa})}{W^{0.067}}$$

The rolling velocity can be calculated by (for $\dot{\phi}_{or} = 0$)

$$U = (\dot{\phi}_{ir} - \dot{\phi}_b) \frac{(d_p - D_b \cos\alpha_0)}{2}$$

$$\text{since } \dot{\phi}_b = \frac{(d_p - D_b \cos\alpha_0)}{2\, d_p} \dot{\phi}_{ir}$$

$$U = \frac{d_p^2 - (D_b \cos\alpha_0)^2}{4\, d_p} \dot{\phi}_{ir}$$

Due to the high rolling speed, the films have substantial thickness. For speeds from 0 to 15,000 rpm, the central film thicknesses are shown in Fig.6-15.

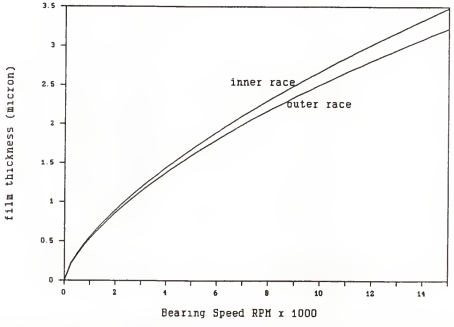

Figure 6-15 Film thicknesses for Bearing A at different speeds and under 1000 N preload.

Temperature Distribution in the Lubricating Film

The following data are used in the temperature calculation:

Material properties of ball, race and lubricant:

for steel ball and race,

ρ = 7800 kg/m^3

C = 470 J/kg °C

k_s = 43 W/m °C

for lubricant,

ρ = 800 kg/m^3

C = 2000 J/kg

k_l = 0.14 W/m

Coefficient of friction:

The coefficient of friction is assumed to be 0.054.

Temperature Rise Inside the Contact Caused by Ball Spinning

The following condition occurs in the inner race contact of Bearing A when it operates at 10,000 rpm.

Q = 163.7

u_r (rolling speed) = 29.8 m/sec

h = 2.6 μm

ω_s (spinning speed) = 938.1 rad/sec

a = 0.8259 mm, b = 0.0938 mm.

The ball spinning speed creates the sliding speeds in the contact as shown in Fig.6-16.

Using the above spinning speed, Eq.(4-4), and Eq.(4-6), the temperature distribution inside the inner race EHD contact is plotted in Fig.6-17 and Fig.6-18. The maximum temperature occurs at $\bar{x} = \pm 0.65$ a and $\bar{y} = 0.25$ b. The temperature is calculated at the mid-plane of the film. It also can be found that the calculated film temperature is much higher than the surface temperature. This is because the conductivity of the lubricant is only 0.3% of the metal.

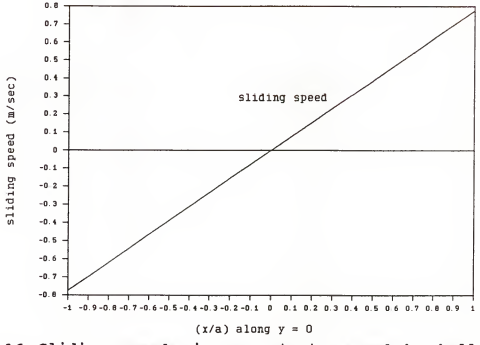

Figure 6-16 Sliding speeds in a contact caused by ball spinning: ω_s = 938.1 rad/sec, a = 0.8259 mm (for Bearing A at 10,000 RPM).

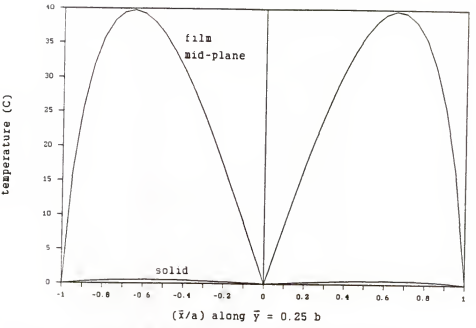

Figure 6-17 Film temperature distribution along $\bar{y}$ = 0.25 b (transverse direction), resulting from the spinning in Fig.6-16 (Bearing A under 1,000 N preload).

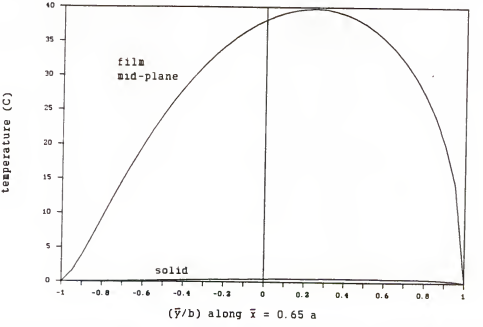

Figure 6-18 Film temperature distribution along $\bar{x}$=0.65 a (rolling direction), resulting from the spinning in Fig.6-16 (Bearing A under 1,000 N preload).

Traction Curves Considering the Thermal Effects

In order to determine the effects of sliding inside the EHD contact, two traction curves are calculated by using the following parameters:

1) limiting shear stress = 0.054 P.

2) no limiting shear stress

Lubricant viscosity model:

η (viscosity at 40° C) = 0.08 Pa·s

α (viscosity-pressure factor) = 2.0×10^{-8} (1/Pa)

β (viscosity-temperature factor) = 0.04 (1/°C)

Other parameters:

h = 2.6 μm

U (rolling speed) = 30 m/sec

b = 0.1 mm

The values of ρ C k are the same as that specified earlier.

The procedure used in the calculation of traction coefficient is outlined in the flow chart in Fig.3-3. The maximum values of the two traction curves in Fig.6-19 occur when the sliding speed is about 0.2 m/sec. It can be found that the limiting shear stress significantly affects the maximum value of the traction coefficient. The two traction curves exhibit negative slopes at high sliding speeds.

Effects of the Shape of the Traction Curve

To investigate how the variation of the traction curve affects the ball skidding phenomenon, time simulations are performed on the following three assumed traction curves (in Fig.6-20):

Curve 1: $u_m = 0.2$ m/sec, $\mu_0 = 0$, $\mu_m = 0.054$, $\mu_f = 0.054$

Curve 2: $u_m = 0.2$ m/sec, $\mu_0 = 0$, $\mu_m = 0.075$,
$\mu_f = 0.035$ (when sliding $\geq$ 3 m/sec)

Curve 3: $u_m = 0.2$ m/sec, $\mu_0 = 0$, $\mu_m = 0.075$,
$\mu_f = 0.035$ (when sliding $\geq$ 2 m/sec)

The heat generation rates on Bearing B at 9,500 rpm corresponding to the above three traction curves are presented in Fig.6-21. It has been shown in Fig.6-6 that Traction Curve 1 will lead to ball skidding. An interesting result is that the minor difference between Traction Curves 2 and 3 creates a large difference in the heat generation rate (in Fig.6-21). This is because only the traction coefficients in the range between 0.5 m/sec to 2 m/sec are really important to the ball skidding, due to the ball spinning.

It also can be found that the negative slope in the traction curve does not have significant effects on the ball skidding phenomenon.

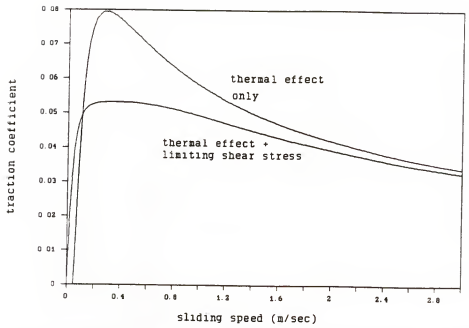

Figure 6-19 Calculated traction curves (using Roelands viscosity): in one curve, the limiting shear stress is assumed to be 0.54 p; in another curve, there is no limiting shear stress.

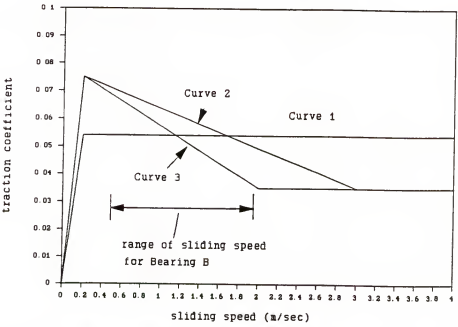

Figure 6-20 Assumed three traction curves for investigating how the shape of traction curve affects ball skidding.

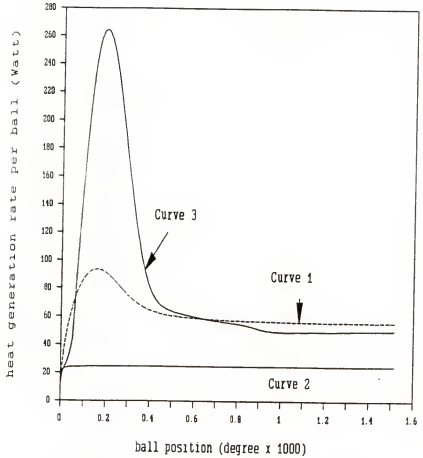

Figure 6-21 Heat generation rates calculated according to the three traction curves in Fig.6-20. The minor difference between Traction Curves 2 and 3 results in a significant difference in heat generation rate. This result shows that the traction coefficients in the thermal region is important to the ball skidding. The initial transient variation should be ignored.

Film Temperature and Estimated Bulk Temperature

The heat generation rates in Bearing A and Bearing B at different speeds have been shown in Fig.6-8. It is also desirable to know the temperatures in EHD films resulting from the calculated heat generation rates.

Bulk bearing temperature . It is extremely difficult to calculate the bulk bearing temperature, thus this temperature is estimated by assuming that all the heat is taken away by a lubricant flow of 0.1 liter/min. The bulk bearing temperature is calculated by

$$T_{bulk} = \frac{\dot{H}}{\rho_{oil}\, C_{oil}\, Q} + T_{oil} \qquad (4\text{-}1)$$

This estimation method gives bulk bearing temperatures that are close to the true measured values from bearing outer races.

Film temperature. For Bearing A, the calculated temperature rise in the lubricating film is 40°C at 10,000 rpm, and the estimated bulk temperature is 30°C (Fig.6-22). There shouldn't be significant lubricant deterioration occurring due to this temperature.

The temperature rise in Bearing B caused by ball skidding is shown in Fig.6-23. Due to the high heat generation rate (57 Watts per ball), very high temperatures (435°C bulk temperature and 930°C film temperature) result. Note that the

bulk temperature of this bearing at 6,000 rpm is 20°C which corresponds to the measured outer race temperature.

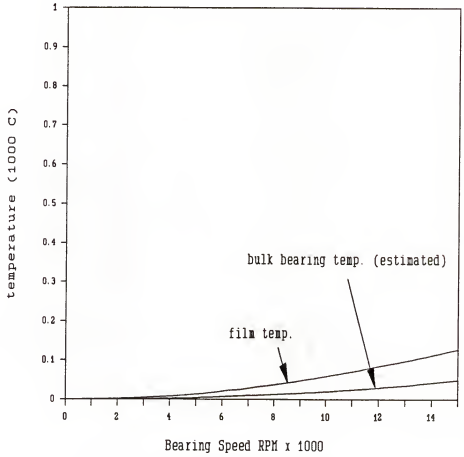

Figure 6-22 Temperature rises in Bearing A. Heat is carried away by an 0.1 lit/min oil flow.

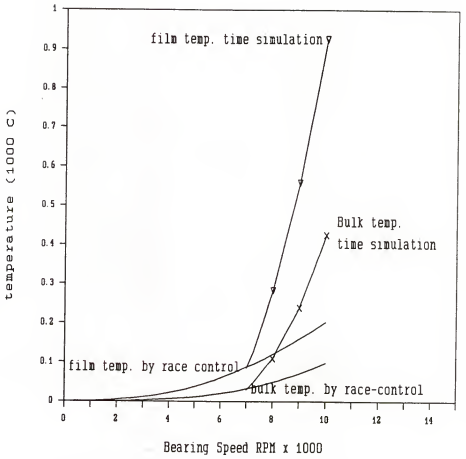

Figure 6-23 Temperature rises in Bearing B. Heat is carried away by an 0.1 lit/min oil flow.

CHAPTER 7
SUMMARY AND CONCLUSIONS

Based on a bearing dynamic analysis, the ball motion and heat generation rates in a 60° and a 15° contact angle ball bearings are calculated. The major purpose of this investigation is to explain the sudden failure of the 60° contact angle ball bearing in a machine tool spindle. Some important results are:

1. The time-simulation results on Bearing B (60° contact angle) show that when the bearing is accelerated from the 8,500 rpm to 9,500 rpm, the heat generation rate almost doubles - from 32 Watts to 57 Watts per ball. According to the calculated heat generation rates, if the bulk temperature of Bearing B at 6,000 rpm is 20°C (in fact, this is the temperature measured at the Bearing B outer race), the bulk temperature at 9,500 rpm with the same lubricant flow rate will be 435°C. If the bearing is non-axisymmetrically loaded, the temperature will be even higher.

   It is hard to pinpoint at which temperature the seizure will occur. Since the AISI M series steels (the common bearing materials) begin to soften at 400°C, it can be expected that large deformation of the balls can be caused

by the compressions between the balls and races when the temperature is above this value.

2. It can be found that the ball spinning decreases the threshold speed of ball skidding in two ways. First, the ball spinning takes away some of the available traction force at the inner race contact. This is the reason why ball skidding actually occurs in Bearing B at speeds lower than 9,000 rpm which was predicted without considering the combined effect of the ball spinning and ball skidding. Second, the heat generation caused by the ball spinning diminishes the traction coefficient. It was shown that the magnitude of the traction curve in the thermal region is important to the threshold speed of ball skidding. It was also found that the negative slope of the traction which may sometimes cause self-excited motion does not affect the ball skidding phenomenon.

3. The ball skidding generates much more heat than the ball spinning does. The heat generation rates in Bearing B calculated by time simulations are about five times that calculated by race-control theory which only considers the ball spinning. The heat generation rate in Bearing B (60° ball bearing) is also much higher than that in Bearing A (57 Watts per ball at 9,500 rpm in Bearing B compared to 2.62 Watts heat per ball at 10,000 rpm in Bearing A).

4. From a thermal analysis, the temperature in the EHD film caused by the 2.62 Watts heat rate is 40°C above the metal

surface temperature (rolling speed is 30 m/sec). There is only a small increase (0.8°C) of the temperature on the metal surface in the contact area. The difference is due to the fact that lubricant thermal conductivity is usually only 0.3% of that of metal.

5. Ball skidding phenomenon is a typical example showing that traction coefficient is related to the stability of motion. In fact, there are many instances in the physical world (eg., skidding at the traction-driving contacts, stick-slip motion [30], self-excited cage whirl motion [13,14], etc.) that display this characteristic. Thus, the mathematical modelling technique used in this work should find applications in areas other than ball bearings.

APPENDIX A
HERTZIAN POINT-CONTACT SOLUTIONS

This appendix presents the Hertzian solutions for the contact geometry and pressure distribution between two contacting elliptic bodies.

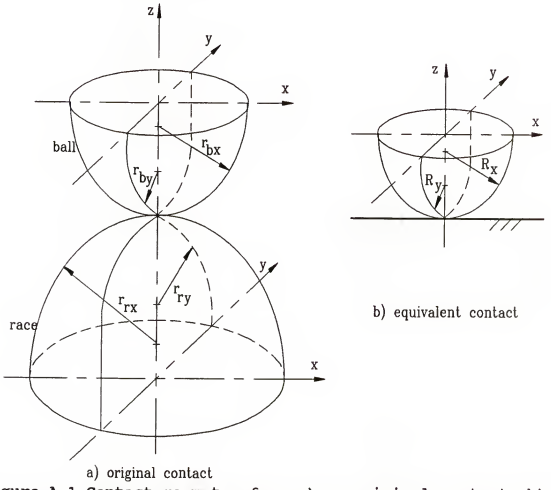

Figure A-1 Contact geometry for: a) an original contact; b) the equivalent contact.

Equivalent Radius for Two Elliptic Bodies in Contact

When two elliptical bodies are brought together into contact as shown in Fig.A-1a, the contact geometry can be represented by an equivalent elliptical body near a plane as in Fig.A-1b. The geometric separation between the two original elliptical bodies is the same as the separation between the equivalent body and the plane. At a point (x,y), the geometric separation can be written as

$$S(x,y) = \frac{x^2}{2\,R_x} + \frac{y^2}{2\,R_y} \qquad \text{(A-1)}$$

In deriving the above expression, the following approximation has been employed:

$$R_x - \sqrt{R_x^2 - x^2} = R_x - \left(R_x - \frac{x^2}{2\,R_x} + \ldots \right)$$

Since the contact region is usually small, the above approximation has sufficient accuracy. A similar approximation for R_y has also been used.

The radius of the equivalent elliptical body can be calculated by

$$\frac{1}{R_x} = \frac{1}{r_{xb}} + \frac{1}{r_{xr}} \qquad \text{(A-2a)}$$

$$\frac{1}{R_y} = \frac{1}{r_{yb}} + \frac{1}{r_{yr}} \qquad \text{(A-2b)}$$

$$\frac{1}{R} = \frac{1}{R_x} + \frac{1}{R_y} \qquad \text{(A-2c)}$$

where R_x, R_y are the equivalent radii in the x-direction and y-direction respectively

R is the over all equivalent radius

r_{bx} and r_{by} are the radii of the ball in the planes containing x-axis and y-axis respectively,

r_{cx} and r_{cy} are the radii of race curvature in the planes containing x-axis and y-axis respectively.

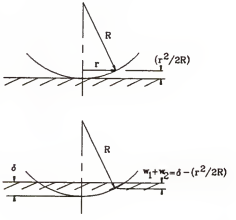

Figure A-2 Deformation on a sphere when it is pressed into a semi-infinite surface.

Elasticity Theory

For calculating the elastic deformation caused by an applied load, the following equation presented by Timoshenko and Goodier [29] can be applied. This equation specifies the deformation at a point on a semi-infinite surface caused by a pressure p acting on a small area dA from a distance r.

$$d\delta = \frac{2\ p\ (1-\nu^2)}{\pi\ E'r}\ dA \qquad (A-3)$$

or

$$\delta = \frac{2\ p}{\pi\ E'} \int\int \frac{dx_1\ dy_1}{\sqrt{(y-y_1)^2 + (x-x_1)^2}} \qquad (A-4)$$

where E' is defined as $E/(1-\nu^2)$, the elastic modulus, and ν is the Poison's ratio.

Hertzian Pressure Distribution

As shown in Fig.A-2, an elliptical body is pressed into a semi-infinite surface by a distance δ. The deformation of a point at a distance r from the center point can be expressed as

$$w_1 + w_2 = \delta - \frac{x^2}{2\ R_x} - \frac{y^2}{2\ R_y} \qquad (A-5)$$

where w_1 and w_2 represent the deformation on the elliptical body and the plane respectively. It was found by using Eq.(A-5) that the pressure distribution which engenders such deformation is

$$\sigma = \frac{3Q}{2\pi ab}\ [\ 1 - (\frac{x}{a})^2 - (\frac{y}{b})^2\ ]^{1/2} \qquad (A-6)$$

Then, the maximum pressure of the contact is

$$P_{max} = \frac{3Q}{2\pi ab} \qquad (A-7)$$

where a is the semi-major axis of the contact ellipse, and b is the semi-minor axis of the contact ellipse.

Hertzian Solution for the Point-Contact Application

Harris [1] has summarized the solutions for the contact and deflection for the application of ball bearings as follows:

$$a = \left(\frac{3}{E'}\right)^{1/3} a^* \left(Q R \right)^{1/3} \tag{A-8}$$

$$b = \left(\frac{3}{E'}\right)^{1/3} b^* \left(Q R \right)^{1/3} \tag{A-9}$$

elastic deformation

$$\delta = \left(\frac{3}{E'}\right)^{2/3} \delta^* \frac{Q^{2/3}}{2 R^{1/3}} \tag{A-10}$$

Eq.(A-10) can be rewritten in the form of Eq.(3-2) as

$$Q = K \delta^{3/2}$$

and $$K = \left(\frac{E'}{3}\right) \frac{2 R^{1/2}}{\delta^{*3/2}} \tag{A-11}$$

where E′ is defined as:

$$E' = \frac{E}{1 - \nu^2} \tag{A-12}$$

The constants a*, b*, and δ^* are defined as

$$a^* = \left(\frac{2 \kappa^2 E_2}{\pi} \right)^{1/3} \tag{A-13a}$$

$$b^* = \left(\frac{2\,E_2}{\pi\,\kappa} \right)^{1/3} \qquad \text{(A-13b)}$$

$$\delta^* = \frac{2\,E_1}{\pi} \left(\frac{\pi}{2\,\kappa^2\,E_1} \right)^{1/3} \qquad \text{(A-13c)}$$

Where R is the equivalent radius of the elliptic contact as defined earlier, and κ is the ellipticity ratio defined as

$$\kappa = \frac{a}{b} \qquad \text{(A-14)}$$

E_1 is the complete elliptical integration of the first kind

$$E_1 = \int \frac{1}{\sqrt{[1-\,(\,1-\,b^2/a^2\,)\,\sin^2\phi]}}\, d\phi \qquad \text{(A-15a)}$$

and E_2 is the complete elliptical integration of the second kind

$$E_2 = \int \sqrt{[1-\,(\,1\,-b^2/a^2\,)\,\sin^2\phi]}\; d\phi \qquad \text{(A-15b)}$$

In the above equations, the ratio κ is an unknown which has to be determined by solving the following equation:

$$\frac{(\,\kappa^2 + 1\,)\,E_2 - 2\,E_1}{(\,\kappa^2 - 1\,)\,E_2} = F(R) \qquad \text{(A-16)}$$

where, F(R) is defined as

$$F(R) = \left[\left(\frac{1}{r_{bx}} - \frac{1}{r_{by}} \right) + \left(\frac{1}{r_{rx}} - \frac{1}{r_{ry}} \right) \right] R$$

Curve-Fitting Formulas for Elliptic-Contact Deformation:

Harris [1] has solved Eq.(A-16), and he presented the solutions in tables. A simpler method to obtain the values of κ, E_1, and E_2 is to use the equations derived by Brewe and Hamrock (1977) as shown below. These equations are obtained by using curve-fitting with the least square method.

$$\kappa = 1.0339 \left(\frac{R_x}{R_y} \right)^{0.6360} \tag{A-17a}$$

$$E_1 = 1.5277 + 0.6023 \ln(R_x / R_y) \tag{A-17b}$$

$$E_2 = 1.0003 + \frac{0.5968}{(R_x/R_y)} \tag{A-17c}$$

APPENDIX B
EHD LUBRICATION THEORY

Since the mid-20 century, the elastohydrodynamic lubrication phenomenon has been intensively studied. It is now commonly known that the development of the EHD film is governed by the following equations:

- .Lubrication action (governed by the Reynolds equation)
- .Elastic theory
- .Lubricant Rheology (variation of lubricant viscosity)
- .Energy equation (determines the temperature distribution and the viscosity in the film)

The Reynolds equation is derived by combining the Navier-Stokes equation and the continuity equation. In deriving the Reynolds equation, the fluid is assumed to be Newtonian and iso-viscous. The Navier-Stokes equations for a Newtonian flow are written as

$$\frac{\partial p}{\partial x} = \frac{\partial}{\partial z}\left(\eta \frac{\partial u}{\partial z}\right)$$

$$\frac{\partial p}{\partial y} = \frac{\partial}{\partial z}\left(\eta \frac{\partial v}{\partial z}\right)$$

The Reynolds equation is derived by using the integral form of the continuity equation:

$$\frac{\partial}{\partial x}\int u\,dz + \frac{\partial}{\partial y}\int v\,dz + \frac{\partial}{\partial z}\int w\,dz = 0$$

Also, according to Fig.B-1, the boundary conditions are

$z = 0,\ u = U_1,\ v = V_1,\ w = W_1$

$z = h,\ u = U_2,\ v = V_2,\ w = W_2$

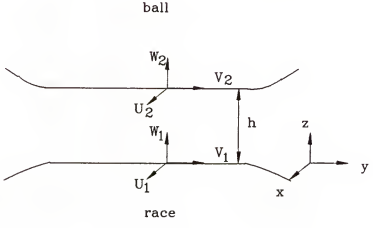

Figure B-1 Coordinate System for deriving the Reynolds equation.

Derivation of the Reynolds Equation

According to the Navier-Stokes equation, the velocity components are in parabolic forms as

$$u = \frac{1}{2\eta}\frac{\partial p}{\partial x} z^2 + C_1 \frac{1}{\eta} z + C_2$$

$$v = \frac{1}{2\eta}\frac{\partial p}{\partial y} z^2 + C_3 \frac{1}{\eta} z + C_4$$

By utilizing the boundary conditions, the constants can be determined. The velocity profiles now can be written as

$$u = -z\left(\frac{h-z}{2\eta}\right)\frac{\partial p}{\partial x} + U_1\left(\frac{h-z}{h}\right) + U_2\frac{z}{h}$$

$$v = -z\left(\frac{h-z}{2\eta}\right)\frac{\partial p}{\partial y} + V_1\left(\frac{h-z}{h}\right) + V_2\frac{z}{h}$$

By substituting the above velocity profiles into the integral form of continuity equation, we arrive at the standard form of Reynolds equation:

$$\frac{\partial}{\partial x}\left(\frac{h^3}{\eta}\frac{\partial p}{\partial x}\right) + \frac{\partial}{\partial y}\left(\frac{h^3}{\eta}\frac{\partial p}{\partial y}\right) = 12(U_1 + U_2)\frac{\partial h}{\partial x} + 12(V_1 + V_2)\frac{\partial h}{\partial y} + (W_1 - W_2) \quad \text{(B-1)}$$

Solution Methods for the Reynolds Equation

Solving the Reynolds equation for the EHD lubrication is difficult due to the following two reasons: 1. a small change in the film shape creates a significant change in the pressure distribution. 2. lubricant viscosity increases with pressure.

Thus, the following procedure which is effective for HD problems but is not applicable in EHD problems.

film shape -> pressure -> deformation ->

film shape -> ...

The above method is known as the forward method which usually does not lead to a convergent solution. It has been suggested that an inverse method should be used in order to avoid the divergence problem. The inverse method utilizes the Reynolds equation to determine film shapes from pressure profiles instead of obtaining pressure profiles from film shapes as in the forward method.

Film Shape

The shape of an EHD film can be written as

$$h(x,y) = h_0 + \delta(x,y) + S(x,y) \qquad \text{(B-2)}$$

where, h_0 is a constant to be determined.

$\delta(x,y)$ is the elastic deformation

$S(x,y)$ is the initial separation which can be written as

$$S(x,y) = \frac{x^2}{2R_x} + \frac{y^2}{2R_y}$$

Determination of Film Shape by the Inverse Method

The purpose of using the inverse method is to obtain a film shape from a prescribed pressure profile. The inverse method needs to use the integrated Reynolds equation (one-dimensional) as,

$$\frac{\partial p}{\partial y} = 12\ \eta\ V\ \frac{h - h_m}{h^3} \qquad \text{(B-3)}$$

where h_m is the film thickness at dp/dy = 0 (maximum pressure point). The integrated Reynolds equation is derived by performing an integration over y.

From the film shape equation, Eq.(B-2), it can be found that when the pressure center (the deformation center) moves forward, the slope of the film shape changes. This fact can be utilized in the selection of the pressure profile in the analysis of the inverse method.

REFERENCES

1. Harris T. A.,"An Analytical Method to Predict Skidding in Thrust-Loaded, Angular-Contact Ball Bearings," Trans. of ASME, J. of Lubrication Technology, Vol. 93, Jan. 1971, p. 17.

2. Harris T. A., "Ball Motion in Thrust-Loaded, Angular Contact Bearings With Coulomb Friction," Trans. of ASME, J. of Lubrication Technology, Vol.93, Jan. 1971, p. 22.

3. Jones, A. B., "Ball Motion and Sliding Friction in Ball Bearings," Trans. of ASME, J. of Basic Engineering. Vol. 81, March 1959, p. 1.

4. Kleckner R. J., "High Speed Cylindrical Roller Bearing Analysis," SKF Computer Program 'CYBEAN'- Vol. 1 Analysis, SKF Report No. AL78P022, July 1978.

5. Hadden G. B., "Steady State and Transient Thermal Analysis of a Shaft Bearing System Including Ball, Cylindrical and Tapered Roller Bearings," SKF Report No. AT81D040 for Program 'SHABERTH,' May 1981.

6. Walters C. T., "The Dynamics of Ball Bearings," Trans. of ASME, J. of Lubrication Technology, Vol. 93, Jan. 1971, p. 1.

7. Gupta P. K., "Transient Ball Motion and Skid in Ball Bearings," Trans. of ASME, J. of Lubrication Technology, Vol. 97, April 1975, p. 261.

8. Gupta P. K., "Frictional Instabilities in Ball Bearings," STLE Tribology Trans., Vol. 31, 2, 1987, p. 258.

9. Poplawski J. V., "Slip and Cage Forces in a High-Speed Roller Bearing," Trans. of ASME, J. of Lubrication Technology, Vol. 94, April 1972, p. 143.

10. Boness R. J., "The Effect of Oil Supply on Cage and Roller Motion in a Lubricated Roller Bearing," Trans. of ASME, J. of Lubrication Technology, Vol. 92, Jan. 1970, p. 39.

11. Pasdari M. and Gentle C. R., "Effect of Lubricant Starvation on the Minimum Load Condition in a Thrust-Loaded Ball Bearing," ASLE Trans., Vol. 30, 3, 1986, p. 355.

12. Kannel J. W. and Snediker D. K., "The Hidden Cause of Bearing Failure," Machine Design, April 7, 1977, p. 78.

13. Kannel J. W., "A Simplified Model of Cage Motion in Angular Contact Bearings Operating in the EHD Lubrication Regime," Trans. of ASME, J. of Lubrication Technology, Vol. 100, July 1978, p. 395.

14. Crawford R.M., "The Dynamics of Ball Separators in Ball Bearings - Part I: Analysis, Part II: Results of Optimization Study," ASLE Trans., Vol. 28, 3, 1984, p. 277.

15. Kawakita K., "Actual Ball Behaviors and the Effect of the Shaft Speed on Ball Motion in a Radial Ball-Bearing," Proceedings of the JSLE International Tribology Conference, July 1985, p. 579.

16. Touma K., "Ball Motion in High-Speed Angular Contact Ball Bearings," Proceedings of the JSLE International Tribology Conference, July 1985, p. 585.

17. Cheng H. S. and Sternlight B., "A Numerical Solution for the Pressure, Temperature and Film Thickness Between Two Infinitely Long, Lubricated Rolling and Sliding Cylinders, Under Heavy Loads," Trans. of ASME, J. of Basic Engineering, Vol. 87, Sep. 1965, p. 695.

18. Kingsbury E. P., "Lubricant-Breakdown in Instrument Ball Bearings," Trans. of ASME, J. of Lubrication Technology, Vol. 100, July 1978, p. 386.

19. Bair S. and Winer W. O., "A Rheological Model for Elastohydrodynamic Contacts Based on Primary Laboratory Data," Trans. of ASME, J. of Lubrication Technology, Vol. 101, July 1979, p. 258.

20. Bair S. and Winer W. O., "Shear Strength Measurements of Lubricants at High Pressures," Trans. of ASME, J. of Lubrication Technology, Vol. 101, July 1979, p. 251.

21. Conry T. F., "Thermal Effects on Traction in EHD Lubrication," Trans. of ASME, J. of Lubrication Technology, Vol. 103, Oct. 1981, p. 533.

22. Houpert L., "New Results of Traction Force Calculations in Elastohydrodynamic Contacts," Trans. of ASME, J. of Tribology, Vol. 107, April 1985, p. 241.

23. Houpert L., "Fast Numerical Calculations of EHD Sliding Traction Forces; Application to Rolling Bearings," Trans. of ASME, J. of Tribology, Vol. 107, April 1985, p. 234.

24. Dalmaz G. and Chaomleffel J. P. "Elastohydrodynamic Lubrication of Point Contacts for Various Lubricants," Proceedings of the 13th Leeds-Lyon Symposium on Tribology, England, Sep. 1986, p. 207.

25. Bair S. and Winer W. O., "Shear Rheological Characterization of Motor Oils," STLE Tribology Trans. Vol. 31, 3, 1987, p. 317.

26. Bezot P. and Hesse-Bezot C., "A Study of Traction in Elastohydrodynamic Lubrication: Experimental and Simulated Curves for a Point Contact Lubricated by a Silicone Fluid," Wear, Vol. 123, 1988, p. 12.

27. Archard, J. F., "The Temperature of Rubbing Surfaces," Wear, Vol. 2, 1959, P. 438.

28. Rashid M. and Seireg A., "Heat Partition and Transient Temperature Distribution in Layered Concentrated Contacts: Part I - Theoretical Model, Part II - Dimensionless Relationships and Numerical Results," ASME/ASLE Joint Tribology Conference, Pittsburgh, PA, October 1986, p. 1.

29. Timoshenko S. P., "Theory of Elasticity," McGraw-Hill, New York, 1972.

30. Maksimov I. L., "Thermal Instability of Sliding and Oscillations Due to Frictional Heating Effect," Trans. of ASME, J. of Tribology, Vol. 110, Jan. 1988, p. 69.

BIOGRAPHICAL SKETCH

Shu-Hsing Chen was born in Tainan, Taiwan, on June 27, 1957. Most of his family members live in Taiwan.

In June, 1979, he received his Bachelor of Science degree in aeronautical engineering from the National Cheng-Kung University, Tainan, Taiwan. In June, 1981, he received his Master of Science degree in engineering science from the same university.

After serving for two years in the military and one year as an instructor in a technological college, he entered the University of Florida in September, 1984, for graduate study toward the Doctor of Philosophy degree.

He is happily married to Shiow-Huey Hsieh.

I certify that I have read this study and that in my opinion it conforms to acceptable standards of scholarly presentation and is fully adequate, in scope and quality, as a dissertation for the degree of Doctor of Philosophy.

Donald W. Dareing, Chair
Professor of Mechanical Engineering

I certify that I have read this study and that in my opinion it conforms to acceptable standards of scholarly presentation and is fully adequate, in scope and quality, as a dissertation for the degree of Doctor of Philosophy.

Jiri Tlusty
Graduate Research Professor of Mechanical Engineering

I certify that I have read this study and that in my opinion it conforms to acceptable standards of scholarly presentation and is fully adequate, in scope and quality, as a dissertation for the degree of Doctor of Philosophy.

Daniel C. Drucker
Graduate Research Professor of Aerospace Engineering, Mechanics, and Engineering Science

I certify that I have read this study and that in my opinion it conforms to acceptable standards of scholarly presentation and is fully adequate, in scope and quality, as a dissertation for the degree of Doctor of Philosophy.

Gary K. Matthew
Associate Professor of Mechanical Engineering

I certify that I have read this study and that in my opinion it conforms to acceptable standards of scholarly presentation and is fully adequate, in scope and quality, as a dissertation for the degree of Doctor of Philosophy.

George Piotrowski
Associate Professor of
Mechanical Engineering

This dissertation was submitted to the Graduate Faculty of the College of Engineering and to the Graduate School and was accepted as partial fulfillment of the requirements for the degree of Doctor of Philosophy.

December, 1989

for Winfred M. Phillips
Dean, College of
Engineering

Madelyn M. Lockhart
Dean, Graduate School